https://doi.org/10.1016/j.phymed.2020.153413



# Icariin ameliorates estrogen-deficiency induced bone loss by enhancing IGF-I signaling via its crosstalk with non-genomic ERα signaling

Liping Zhou[a#], Christina Chui-Wa Poon[a#], Ka-Ying Wong[a], Sisi Cao[a], Xiaoli Dong[a], Yan Zhang[a,c*], Man-Sau Wong[a,b*]

[a]Department of Applied Biology and Chemical Technology, The Hong Kong Polytechnic University, Hung Hom, Kowloon, Hong Kong SAR.

[b]State Key Laboratory of Chinese Medicine and Molecular Pharmacology (Incubation), The Hong Kong Polytechnic University Shenzhen Research Institute, Shenzhen, PR China.

[c]Longhua Hospital, Shanghai University of Traditional Chinese Medicine, Shanghai, PR China.

Running title: Icariin induced osteogenesis via IGF-IR-ERα crosstalk

[#]Co-first authors with equal contribution.

[*]*Co-Correspondence:*

Prof. Man-Sau Wong

Email: man-sau.wong@polyu.edu.hk

Room Y806, The Hong Kong Polytechnic University, Hung Hom, Kowloon, Hong Kong SAR.

Phone: (852)-34008665; Fax: (852)-23649932

Dr. Yan Zhang

Email: medicineyan@usst.edu.cn

Longhua Hospital, Shanghai University of Traditional Chinese Medicine, Shanghai, PR China

Phone: (21)-64385700

## Abstract

***Background:*** Rapid, non-genomic estrogen receptor (ER) signaling plays an integral role in mediating the tissue selective properties of ER modulators. Icariin, a bone bioactive flavonoid, has been reported to selectively activate non-genomic ERα signaling in *in vitro* and *in vivo* studies.

***Purpose:*** The mechanisms underlying the estrogen-like bone protective effects of icariin are not fully understood, especially those that are related to insulin-like growth factor I (IGF-1) signaling. The bone protective effects of icariin were investigated in female mature ovariectomized (OVX) rats and the signaling of IGF-IR- ERα cross-talk was determined in osteoblastic cells.

***Study design and methods:*** Icariin at 3 different dosages (50, 500 and 3000 ppm) were orally administrated to rats for 3 months through daily intake of phytoestrogen-free animal diets containing icariin. Bone marrow stromal cells (BMSCs) and osteoclast precursors from femurs were harvested for experiments and RNA-sequencing. The interactions between IGF-IR and non-genomic ERα signaling were examined in pre-osteoblastic MC3T3-E1 cells and mature osteoblasts differentiated from BMSCs.

***Results:*** Our results show that chronic administration of icariin to OVX rats significantly protected them against bone loss at the long bone and lumbar spine without inducing any uterotrophic effects. *Ex vivo* studies using BMSCs and osteoclast precursors confirmed the stimulatory effects of icariin on osteoblastogenesis and its inhibitory effects on osteoclastogenesis, respectively. RNA-sequencing analysis of mRNA from BMSCs revealed that icariin at 500 ppm significantly altered IGF-1 signaling as well as PI3K-Akt pathways. Our results demonstrated for the first time the rapid induction of interactions between IGF-IR and ERα as well as IGF-IR signaling and the downstream Akt phosphorylation by icariin in MC3T3-E1 cells. The activation of ERα and Akt phosphorylation by icariin in MC3T3-E1 cells and the osteogenic effects of icariin on ALP activity in mature osteoblasts were shown to be IGF-IR-dependent.

***Conclusion:*** Our findings reveal that icariin activates both ERα and Akt via enhancing rapid induction of IGF-1 signaling in osteoblastic cells for osteogenesis and might be regarded as a novel pathway-selective phytoestrogen for management of postmenopausal osteoporosis.

**Keywords:** icariin; IGF-IR- ERα cross-talk; osteogenesis; pathway-selective phytoestrogens

**Abbreviations:** ER, estrogen receptor; ERE, estrogen response element; PI3K, phosphatidylinositol 3-kinase; IGF-IR, insulin-like growth factor I receptor; KEGG, Kyoto Encyclopedia of Genes and Genomes; BMSCs, bone marrow stromal cells; SERMs, selective estrogen receptor modulators; OVX, ovariectomized; PINP, N-terminal propeptide of type I procollagen; DPD, deoxypyridinoline; MAPK, mitogen activated protein kinase; HEP, *Herba Epimedii*; JNK, c-jun N terminal kinase; DEGs, differentially expressed genes

## Introduction

There is compelling evidence from human intervention studies that estrogen is the dominant sex steroid regulating bone metabolism in both women and men (Khosla and Monroe, 2018). The major cause of osteoporosis for women is the onset of estrogen deficiency following menopause (Riggs et al., 2002), and for men it is the decline in bioavailable estrogen levels that contributes to the development of age-related bone loss (Khosla et al., 2008).

The effects of estrogen are mediated by estrogen receptors (ERα and ERβ) via classical genomic pathways in which ER-ligand complex alters estrogen response element (ERE)-dependent or -independent target genes transcription. Recent studies further indicated that ERs can be activated rapidly (from a few seconds to a few minutes) by estrogen at the cell membrane via extra-nuclear estrogen signaling (Arnal et al., 2017) or ligand-independently by cross-talk with growth factor receptors (such as IGF-IR) which phosphorylates ERs by inducing kinases such as mitogen-activated protein kinase (MAPK) and phosphoinositide 3-kinase (PI3K) (Kato et al., 1995). Indeed, the positive effects of estrogen on bone mass are believed to be mediated by ERα (Khalid and Krum, 2016) via extra-nuclear or membrane-initiated signaling pathways (Bartell et al., 2013; Gustafsson et al., 2016; Manolagas et al., 2013).

Estrogen supplementation with or without progesterone as part of hormone replacement therapy (HRT) could effectively reduce the risk of bone fractures in postmenopausal women (Rossouw et al., 2002), but its use has been limited in recent years due to the concern of the associated risk of reproductive cancers (Nyirjesy, 2003). Specific selective estrogen receptor modulators (SERMs) have been clinically developed to protect against breast cancer without compromising their protective effects on bone (Mirkin and Komm, 2013). However, the agonist/antagonist profiles of these agents require further improvement as they have been shown to exert various undesirable effects on the uterus (tamoxifen) (Glurich et al., 2013) and the cardiovascular system (raloxifene) (Barrett-Connor et al., 2006). With the discovery of the differential actions of nuclear and membrane ERα initiated pathways, a new generation of SERMs with improved tissue specificity can be developed (Gustafsson et al., 2016). Specifically, an ideal bone bioactive SERM will be one that can differentially activate membrane initiated but not nuclear ER signaling pathway, thereby maintaining the beneficial effects of estrogen in bone while avoiding any undesirable effects on other organ systems.

Icariin is a major flavonoid glucoside isolated from *Herba Epimedii* (HEP), the most frequently prescribed herb for clinical management of bone diseases in China (Arnal et al., 2017; Xiao et al., 2014). Both preclinical and clinical studies (Wang et al., 2018; Zhang et al., 2007) showed that icariin is the bioactive compound that accounts for the osteoprotective effects of HEP. Icariin was previously shown by us to exert estrogen-like protective effects on bone in ovariectomized (OVX) mice without inducing any uterotrophic effects and that its estrogenic effects in rat osteoblastic cells were ER-dependent and ERE-independent (Mok et al., 2010). Our recent study (Ho et al., 2018) further showed that icariin induced rapid phosphorylation of ERα at Ser118 and at Ser167 in osteoblastic cells via MAPK/ERK and PI3K/Akt signaling pathways, respectively. Most importantly, the study showed that icariin induced osteogenic and anti-apoptotic effects by selectively activating rapid membrane-initiated ERα signaling pathways in osteoblastic cells, suggesting that icariin behaved as a pathway-selective SERM. However, as icariin is not a ligand of ERs, and the mechanism by which it elicits estrogen-like bone protective actions is far from clear.

Various mechanisms of actions that mediate the ER-dependent bone protective effects of icariin *in vitro* have been reported by others, including ER/ERK/c-jun N terminal kinase (JNK)/p38 (Song et al., 2013; Wu et al., 2017) as well as ER/Wnt/β-catenin (Wei et al., 2016). Here, we

characterized the dose-dependent bone protective effects of icariin on OVX rats, and its ability to induce osteoblastogenesis and osteoclastogenesis as revealed *ex vivo* by bone marrow stromal cells (BMSCs) isolated from icariin-treated rats. We also studied the transcriptional profiles of BMSCs to delineate the mechanism of actions involved in mediating the *in vivo* bone protective effects of icariin. Our results revealed that IGF-IR signaling and its cross-talk with ERα and Akt were enhanced by icariin in osteoblastic cells and this might account for the behavior of icariin as a pathway-selective SERM in stimulating osteogenesis.

## Materials and methods

### *Preparation of control diets containing icariin and Animal study*

Icariin was purchased from Shanghai Winherb Medical Technology Co. Ltd. (http://www.winherb.cn/Index.html) and the purity is 99.3% (CAS#489-32-7, Shanghai, China) and added into diets at three different dosages formulated by Research Diet, Inc (New Brunswick, USA). The present experiment was conducted under an animal license issued by Department of Health, Hong Kong Special Administrative Region Government, and the Hong Kong Polytechnic University Animal Subjects Ethics Sub-committee (ASESC Case: 13/18). Seventy 6-month-old female Sprague-Dawley rats weighing 230±20g were purchased from The Chinese University of Hong Kong and housed in Centralized Animal Facilities (CAF) of The Hong Kong Polytechnic University on a 12h light/dark cycle. Water and food were available *ad libitum*. After one week of acclimatization, all the rats were given bilateral ovariectomy or sham operation. During the preliminary experiment, rats were allowed to take diets freely and the daily amount of intake was recorded for five days. Based on the preliminary study, the mean daily intake of diet for each rat was established as 15g (the minimal amount of daily intake) in the present study. Upon recovery for 2 weeks, the OVX rats were randomly subjected to oral administration with vehicle, 17β-estradiol (E2) (1.0 mg/kg.day) or raloxifene (1.0 mg/kg.day) as well as icariin at three dosages of 50 ppm (D15061901, 0.05g of icariin in 1 kg of diet), 500 ppm (D15061902, 0.5g/kg) or 3000 ppm (D15061903, 3.0 g/kg) in the form of icariin-containing diets for 12 consecutive weeks. During the whole recovery and treatment periods, the rats in the sham, OVX, 17β-estradiol and raloxifene treatment groups were paired-fed with the control phytoestrogen-free diet (AIN-93M, D00031602) to remove any influences of phytoestrogens.

The ingredients of diets have been provided in the supplementary. One day before sacrifice, the animals were housed individually in a metabolic cage for collection of urine. The rats were sacrificed under anesthesia by ketamine/xylazine and blood was collected from the abdominal aorta. The uterus was freshly isolated and weighed. The whole left leg and spine were collected for micro-computed tomography (μ-CT) analysis. The right femur was dissected at sterile conditions for isolation of BMSCs and osteoclast precursors. The right tibia was freshly collected and stored at -80℃ after removal of all soft tissues.

## Chemicals

Chemical compounds studied in this article were Icariin (PubChem CID: 5318997) and picropodophyllin (PubChem CID: 72435).

### *Biochemical assay of serum and urine samples*

Calcium and phosphorus levels in serum and urine as well as urinary level of creatinine were measured using the Arsenazo III UV method with an automatic analyzer HITACHI7100. The kits were purchased from Shanghai Kehua Bio-Engineering Co. Ltd (Shanghai, China). Urinary deoxypyridinoline (DPD) was determined using an enzyme immunoassay DPD EIA kit (QUIDEL Corporation, USA) and normalized by urinary creatinine. Serum level of PINP was measured by ELISA kit (Immunodiagnosticsystems, UK).

### *Micro-computed tomography (Micro-CT) measurements*

Bone properties of the trabecular bone and cortical bone at the proximal tibia and distal femur as well as lumbar vertebra were determined by Micro-CT (μCT40, Scanco Medical, Switzerland) as previously described (Zhou et al., 2018). Briefly, the source energy selected for this study was 70 KVp and 114 μA with a resolution of 21 um. Approximately 200 slices were done for each scan. The distal/proximal were defined as 4.2 mm and 2.2 mm away from the femur/tibia head. Scanning was done at the metaphyseal area located 0.63 mm below the lowest point of the epiphyseal growth plate and extending 2.0 mm in the proximal direction. Bone mineral density (BMD, $mg/cm^3$) and bone morphometric properties, including bone volume over total volume (BV/TV), trabecular bone number (Tb.N, $mm^{-1}$), trabecular bone thickness (Tb.Th, mm), trabecular bone separation (Tb.Sp, mm), connective density (Conn.D, $1/mm^3$) and structure

model index (SMI), were evaluated by contoured VOI images. The bone porosity of the femur and tibia were measured as described by (Britz et al., 2010). The condition was standardized to 100 kVp and 100 μA with a resolution of 3 μm. A 1 mm diameter of circular region of interest (ROI) was selected on the periosteal surface of the anterior part of the bone. The percentage of bone porosity (Cr.Po) (canal volume fraction) was measured.

***Isolation and differentiation of bone marrow stromal cells (BMSCs)***

The isolation and culturing of rat BMSCs were performed according to the methods described in (Chen et al., 2010; Li et al., 2014; Taylor et al., 2014). Briefly, the right femurs from the rats of each treatment group were dissected at sterile conditions and then washed with warm HBSS containing 3% of 100U/ml penicillin/streptomycin (Gibco, USA). After removing the epiphyses, the bone marrow was flashed with Dulbecco's modified medium containing 10% fetal bovine serum, 100U/ml penicillin/streptomycin and 1% amphotericin B (Gibco, USA) into a sterile Petri dish first using a syringe with a 21-gauge needle, followed by a 25-gauge needle. The isolated bone marrow samples were made into a single cell suspension and centrifuged. After the supernatant was discarded, the cells were resuspended for incubation at 37℃ in a 5% $CO_2$ incubator and the culture medium was replaced every 2-3 days. An osteogenic medium containing 10 mM β-glycerophosphate, 50 μg/ml ascorbic acid (Gibco, USA) and 10 nM dexamethasone was applied when osteoblast differentiation was promoted.

***Alkaline Phosphatase (ALP) staining and ALP assay, Alizarin red and Von Kossa staining***

BMSCs were seeded in a 12-well plate at a density of $1.5 \times 10^6$/well and cultured in an osteogenic medium. ALP staining was conducted by following the manufacturer's instruction (Cat#SCR004, Millipore, USA) to evaluate the osteogenic activities of BMSCs on days 10 and 25, respectively. The number of colonies of osteoblast (red/purple) was counted for statistical analysis. ALP activity assay was conducted by the cell at density of $1.5 \times 10^6$/well and cultured in osteogenic medium. ALP staining was conducted by following the manufacturer's instruction (Cat#295-58601, LabAssay™ ALP, WAKO, Japan) to evaluate the ALP activities of mature osteoblasts on day 25. For Alizarin red and Von Kossa staining, the cells were fixed with 4% paraformaldehyde for 10 min at room temperature. The fixed cells were incubated in 2% Alizarin red S (AR-S) solution for 30 min at room temperature followed by washing with Milli-

Q water four times. The amount of $Ca^{2+}$-containing nodule (purple-red spots) was released from the cell matrix by incubation in 10% cetylpyridinium chloride for 15 min. The amount of AR-S dye released was quantified by spectrophotometry at 562 nm and the calcium ion concentration of each sample was normalized to its protein concentration. Von Kossa staining was conducted by incubating the fixed cells with 1% silver nitrate solution for 45 min under UV light at room temperature. After washing four times with Milli-Q water, the cells were treated with 3% sodium thiosulfate for 5 min, washed four times with Milli-Q water, then dried at room temperature. The stained cells were visualized and their images were captured under a light microscope equipped with a digital camera (Olympus, Japan).

***Tartrate-resistant acid phosphatase (TRAP) staining***

The isolation and culturing of osteoclast precursors and osteoclast differentiation were performed according to the methods described in (Chen et al., 2010; Marino et al., 2014). The osteoclast precursors were seeded in a 12-well plate at a density of $2.0 \times 10^6$ per well and cultured in an osteoclastogenic medium containing 10 nM vitamin D3 for 13 days. At the end of the culturing, TRAP staining was conducted by using a commercial kit (Sigma-Aldrich, USA). TRACP-positive osteoclasts containing 3 or more nuclei were regarded as multinucleated osteoclasts and recorded for statistical analysis. The stained cells were visualized and their images were captured under a light microscope equipped with a digital camera (Olympus, Japan).

***RNA sequencing***

RNA sequencing (RNA-seq) was carried out by the Beijing Genomics Institute following standard protocols. The library products were sequenced using BGISEQ-500. Standard bioinformatics analysis was performed by the Beijing Genomics Institute. All the generated raw sequencing reads were filtered by removing reads with adaptors, reads with more than 10% unknown bases, and low quality reads. After filtering, clean reads of each sample (Supplementary Table 2) were mapped to the reference gene by using Bowtie2 program and aligned to the reference genome by using HISAT program. The Q20 and GC contents of the clean data were calculated. All the downstream analyses were based on high-quality clean data. Genes were considered as significantly differentially expressed if their fold changes $\geq 2$ and $<0.5$. Fold change represents the ratio of the expression between two groups. Functions of protein-

coding genes were assigned according to the best match derived from alignments to proteins in the nr (NCBI non-redundant protein sequences) database. Gene Ontology (GO) annotation was performed for all identified DEGs and the WEGO software (Ye et al., 2006) was used to conduct the GO functional classification. GO terms with a P-value ≤0.05 corrected by Bonferroni were defined as significantly enriched GO terms in DEGs. Pathway enrichment analysis of DEGs was performed based on the Kyoto Encyclopedia of Genes and Genomes (KEGG) database (Kanehisa et al., 2008). Raw sequence data are available throughout the NCBI Sequence Read Archive and the accession number of SRA for the submission is PRJNA648394.

After isolation of BMSCs, the femoral head was cut off and homogenized in Trizol reagent by using Precellys 24 homogenizer (Bertin, France). Total RNA extraction, reverse transcription and real-time quantitative PCR assay were carried out as previously described for validation of gene expressions of RNA-seq results (Zhou et al., 2018).

***Confocal immunofluorescence analysis***

BMSCs isolated from 5-week-old female SD rats were seeded onto glass coverslips in a 12-well plate and treated with IGF-1 (100 ng/ml), 17β-estradiol (E2, 10 nM) and icariin (0.1 μM) for 10 min in a phenol red-free medium. Upon treatment, cells were washed with PBS and immediately fixed in 4% paraformaldehyde for 15 min at room temperature. After blocking with 1% BSA for 45 min, the cells were incubated with specific primary antibodies (rabbit anti-IGF-IR and mouse anti-ERα, 1:500) overnight at 4℃. The primary antibodies were probed with both Alexa Fluor 488-conjugated anti-rabbit antibody for IGF-IR (shown in green) and Alexa Fluor 594-conjugated anti-mouse antibody for ERα (shown in red) for 1 hr at room temperature followed by Hoechst counter-staining (shown in blue) (Ho et al., 2018). Fluorescence images were captured at mid-plane of cells (oil objective: 60x) by a Leica TCS SPE DMi8 confocal microscope (Leica Microsystems, Wetzlar, Germany). The overall intensities of the fluorescent signals of single cell were quantified using the corresponding Leica Microsystem software station (LAS AF, Leica Microsystems, Germany) and the overlapping of IGF-IR and ERα (shown in yellow) was quantified using the Imaris 9.0 software (Bitplane, USA).

***Culture and treatment of murine MC3T3-E1 cells***

The murine pre-osteoblastic MC3T3-E1 cells (Subclone 4, CRL-2593, ATCC) were cultured with α-MEM containing 10% FBS and antibiotics (1% penicillin/streptomycin) according to the methods described in our previous study (Ho et al., 2018). Cells were seeded in a 6-well plate at a density of 1.2 x $10^5$/well and cultured in an osteogenic medium for 7 days. The medium was then replaced with phenol red-free α-MEM containing 1% charcoal-stripped FBS for another 24h. After that, cells were treated with icariin (0.01 μM, 0.1 μM and 1 μM), E2 (10 nM) and IGF-1 (100 ng/ml) or Des1,3-IGF-1 (10 ng/ml) as positive control in the presence or absence of IGF-IR antagonist JB-1 (10 μM, 1 h pre-treatment, Sigma, USA) or selective IGF-IR kinase inhibitor picropodophyllin (PPP, 0.5 μM, 6 h pre-treatment, Tocris, UK) at several time points.

***Immunoblotting***

Treated MC3T3-E1 cell lysates were collected using the NP-40 buffer supplemented with protease inhibitor (PMSF, 1 mM) and phosphatase inhibitors (1 mM sodium orthovanadate, 10 mM NaF). Immunoblotting was carried out as previously described (Ho et al., 2018). Rabbit anti-phospho-IGF-IR (1:1000, Thermo Fisher Scientific, USA), rabbit or mouse anti-IGF-IR (1:1000, Thermo Fisher Scientific, USA), rabbit anti-phospho-ERα at serine 167 (1:500, Santa Cruz, USA), rabbit or mouse anti-ERα (1:500, Santa Cruz, USA), rabbit anti-phospho-IRS1 at serine 302 and tyrosine 612 (1:1000, Thermo Fisher Scientific, USA), rabbit anti-IRS1 (1:1000, Cell Signaling, USA), rabbit anti-IRS2 (1:1000, Cell Signaling, USA), mouse anti-phospho-Akt at serine 473 (1:1000, Millipore, USA), mouse anti-Akt 1/2/3 (1:500, Santa Cruz, USA) or mouse anti-β actin (1:2000, Thermo Fisher Scientific, USA) were incubated as primary antibodies.

***Co-Immunoprecipitation***

Treated rat BMSC lysates were harvested by trypsinization and washed with PBS, then lysed in IP lysis buffer (Thermo Fisher Scientific, USA) supplemented with 1 mM PMSF. Cell lysates were cleared by centrifugation at 4°C. Equal amounts of total protein between samples were incubated with the pre-washed appropriate protein A/G plus agarose beads (Thermo Fisher Scientific, USA) and mouse anti-IGF-IR antibody (1:100, Santa Cruz, USA) under constant rotation at 4°C overnight. Then, beads were washed four times with Co-IP lysis buffer, and bound proteins were eluted with SDS sample buffer. Samples were resolved by SDS–PAGE for

immunoblotting. For the detection of endogenous interaction between IRS1, IGF-IR and ERα, co-immunoprecipitation was carried out with mouse anti-IGF-IR antibody (1:100, Santa Cruz, USA), followed by immunoblotting with mouse anti-IGF-IR antibody (Santa Cruz, USA), rabbit anti-IRS1 antibody (1:1000, Cell Signaling, USA) and rabbit anti- ERα antibody (1:100, Santa Cruz, USA).

***Statistics***

The data are expressed as mean ± SEM of the values obtained from individual experiments. Statistical comparisons between groups were performed by Student's *t*-test or one-way analysis of variance (ANOVA) followed by Tukey *post hoc* test; n indicates the number of experiments. A difference of $P<0.05$ was considered statistically significant. GraphPad Prism 5.0 was used for statistical analysis (GraphPad software, Inc., USA).

## Results

***Icariin ameliorates estrogen-deficiency bone loss in OVX rats***

We studied the response of six-month-old OVX rats to treatment with phytoestrogen-free diet containing icariin (at 50, 500 or 3000 ppm), raloxifene (Ralo, 1.0 mg/kg.day), 17β-estradiol (E2, 1.0 mg/kg.day) or vehicle for 3 months. All treatments significantly reduced OVX-induced body weight gain (Table 1). E2 and Ralo, but not icariin, significantly induced uterus index in OVX rats (Table 1). E2, Ralo and icariin at 500 ppm significantly suppressed OVX-induced serum N-terminal propeptide of type I procollagen (PINP, a bone formation biomarker) (Fig. 1A) while all treatments significantly suppressed OVX-induced urinary deoxypyridinoline (DPD, a bone resorption biomarker) (Fig. 1B) in rats. Similar to E2 and Ralo, icariin at all 3 dosages significantly improved bone mineral density (BMD) at the distal femur, proximal tibia as well as lumbar vertebra in OVX rats (Fig. 1C). Icariin at 500 ppm and 3000 ppm also mimicked the effects of E2 and Ralo in reducing cortical porosity (a major determinant of overall bone strength (Cooper et al., 2016)) at the distal femur, but not at the proximal tibia in OVX rats (Fig. 1D). Representative micro-CT images of all three measured bone sites (distal femur, proximal tibia and lumbar vertebra L4) from rats in response to different treatments are shown in Supplementary Fig. 1. E2, Ralo and icariin at 3 dosages improved trabecular bone microarchitecture at those 3 sites to different extent (Supplementary Table 1A) and only cortical

BMD of the distal femur is slightly increased by the treatment of icariin at 500 ppm (Supplementary Table 1B).

***Icariin promotes osteoblastogenesis dose-dependently and suppresses osteoclastogenesis in BMSCs***

To investigate the osteogenic activity of icariin, BMSCs isolated from OVX rats treated with icariin were differentiated; followed by evaluation of their effects on *ex vivo* differentiation and bone formation by ALP staining, Alizarin red staining and Von Kossa staining. Cells isolated from OVX rats treated with E2 and icariin were found to have more intense ALP staining than those from OVX rats (Fig. 2A). Quantitative analysis of the intensity indicated that E2 as well as icariin at 50 and 500 ppm, but not 3000 ppm, significantly induced ALP activity (Fig. 2A). The amount of $Ca^{2+}$-containing nodules, as revealed by Alizarin red staining, was markedly higher in BMSCs isolated from E2-treated as well as icariin-treated rats upon 25 days of incubation (Fig. 2B). The effects of E2 and icariin on osteoblastic mineralization were further confirmed by Von Kossa staining on day 25 (Fig. 2C). There was no ALP or Alizarin red staining in BMSCs isolated from Ralo-treated OVX rats (Fig. 2A and 2B). The effects of icariin on osteoclastogenesis were also studied in osteoclast precursors upon induction with osteoclastogenic medium for 13 days. The number of osteoclast-like cells (multinucleated cells) was determined by TRAP staining. E2, Ralo and icariin at all 3 dosages significantly reduced the number of TRAP-positive multinucleated cells formed from osteoclast precursors isolated from OVX rats (Fig. 2D), suggesting that all treatments could reduce osteoclast formation in OVX rats.

***Analysis of differentially expressed genes (DEGs) and the GO enrichment and Kyoto Encyclopedia of Genes and Genomes (KEGG) pathway analysis***

To study the mechanism involved in the mediating of the actions of icariin on osteogenesis, RNA extracted from BMSCs obtained from all treated rats was subjected to RNA-seq. Over twenty-three million raw reads were generated from the RNA-seq analysis and more than 94.5% of which were clean reads with a percentage of Q20base larger than 92.9% (Supplementary Table 2). The heatmap displayed the cluster analysis of DEGs between the comparison groups (Fig. 3A). Based on the *in vivo* and *ex vivo* study of the effects of icariin, OVX rats fed with 500ppm icariin (ICA500) appeared to have benefitted the most from the favorable effects on serum bone

formation markers (PINP), BMD, cortical porosity, osteoblast number and mineralization (versus 50 ppm and 3000 ppm). Thus, subsequent DEGs and pathway analysis were based on the comparison between OVX group and ICA500 group. The scatter plot and volcano plot of OVX versus ICA500 displayed 341 up-regulated DEGs (yellow) and 424 down-regulated DEGs (blue) (Fig. 3B). To further assess the functional roles of the DEGs, gene ontology (GO) enrichment analysis (Fig. 3C) was performed using the WEGO software based on Wallenius' non-central hyper-geometric distribution. The DEGs were divided into three main GO categories: biological process, cellular component and molecular function. The KEGG pathway analysis of DEGs (Fig. 3D) showed the top 20 pathways with the smallest p-values. The results of this analysis showed that the DEGs were significantly involved in pathways of cell adhesion molecules (CAM), regulation of actin cytoskeleton and focal adhesion (p-value <0.05), which are well known to be related to the pathways that mediate the stimulatory action of mechanical loading in bone tissues.

***Icariin alters the expression of DEGs involved IGF-I signaling and Phosphoinositol-3-phosphate kinase (PI3K)-Akt signaling pathway in BMSCs from treated rats***

IGF-IR was previously shown to interact physically with ERα (Sunters et al., 2010) and initiate rapid ligand- and ERE-independent activation of ERα to induce osteogenic responses to mechanical loading in osteoblastic cells (Jessop et al., 2001; Windahl et al., 2013). As KEGG pathway analysis suggested that icariin might mimic the effects of mechanical loading in bone tissues, a list of differential genes involved in bone formation, bone resorption, IGF-I signaling and PI3K-Akt signaling pathways obtained from RNA-seq analysis of BMSCs derived from different rat groups is shown in Table 2. As expected, icariin at all three dosages induced the expression of genes that were involved in bone formation (Runx2 and Bglap) in BMSCs. Our results also indicated that E2, raloxifene and icariin at 500 ppm and 3000 ppm significantly induced IGF-I mRNA expression in BMSCs isolated from OVX rats (Table 2), suggesting that icariin might induce autocrine regulation of IGF-I production in bone tissues. Moreover, E2 and icariin at 3000 ppm down-regulated insulin receptor substrate 1 (IRS1) while icariin at 50 and 500 ppm down-regulated IGF-IR mRNA expression in BMSCs. Furthermore, raloxifene and icariin at 500 ppm, but not E2, could significantly alter genes (Pik3c2g, Pik3r5, Nos3) that were involved in PI3K-Akt signaling pathways in BMSCs from OVX rats (Table 2).

To experimentally validate the expression levels of 3 DEGs involved in the upstream of IGF-I signaling (Igf1r, Irs1 and Irs2) identified from the RNA-seq data, quantitative real-time PCR (qPCR) was performed to detect the mRNA levels of those genes. As shown in Supplementary Fig. 3, the qPCR results confirmed our RNA-seq analysis results, indicating the similar expression tendency in those 3 genes obtained via both methods.

***Icariin rapidly up-regulates insulin-like growth factor I receptor (IGF-IR) expression level and induces the co-localization of IGF-IR and ERα in osteoblastic cells***

To determine if IGF-IR was involved in the mediating of the actions of icariin, its ability to enhance IGF-IR-ERα interactions and IGF-IR signaling in osteoblastic cells was studied. IGF-1 (100 ng/ml) significantly induced IGF-IR (green) protein expression (Fig. 4A and 4B), while icariin (0.1 μM) and E2 (10 nM) significantly increased IGF-IR (green) and ERα (red) protein expression in differentiated BMSCs upon treatment for 10 min (Fig. 4A and 4B). Fig. 4C showed that all three treatments could significantly induce co-localization of IGF-IR and ERα in differentiated BMSCs, as revealed by analysis of the 3D confocal images in Fig. 4A (e-f). To confirm icariin was able to increase the interactions between IGR-IR, ERα and downstream signaling molecule, IRS-1, rat BMSCs were subjected to treatment with either des (1-3) IGF-1 (which do not bind to IGF binding protein) (100 ng/ml), IGF-1 (100 ng/ml) or icariin (0.1 μM). As shown in Fig. 4D, icariin mimicked IGF-1 in inducing the co-immunoprecipitation of IGF-IR, IRS-1 and ERα. These results suggest that icariin indeed enhances the physical interactions between ERα, IGF-IR and its downstream signaling molecules.

***Icariin rapidly activates IGF-IR signaling in MC3T3-E1 cells***

To further determine if IGF-IR signaling cascades were involved in the mediating of the rapid actions of icariin in osteoblastic cells, the effects of icariin (10 nM, 0.1 μM and 1 μM) on the expression of IGF-IR, IRS1, IRS2 as well as the phosphorylation of IGF-IR in murine pre-osteoblastic MC3T3-E1 cells were studied. Icariin at all three dosages significantly up-regulated the IRS1 expression level in 10 min, but not IRS2 (Fig. 5A-C). Moreover, IGF-1 (100 ng/ml), E2 (10 nM) and icariin at 0.1 μM significantly induced IGF-IR phosphorylation in MC3T3-E1 cells within 10 min of incubation (Fig. 5A and 5D). The time-dependent effects of icariin (0.1 μM),

IGF-1 (100 ng/ml) and E2 (10 nM) on IRS-1 phosphorylation at Tyr 612 in MC3T3-E1 cells were also studied (Fig. 5E). IGF-1, but not E2, rapidly induced IRS-1 phosphorylation at Tyr 612 within 1-5 min of incubation while icariin induced IRS-1 phosphorylation at 10 minutes of incubation in MC3T3-E1 cells (Fig. 5F). These results suggest that icariin rapidly enhances IGF-1 signaling by enhancing the expression and phosphorylation of its signaling proteins in osteoblastic cells.

***Blocking of IGF-IR kinase abolishes the phosphorylation of IGF-IR, ERα and the PI3K downstream effector Akt induced by icariin in MC3T3-E1 cells***

To investigate if IGF-IR was involved in the mediating of phosphorylation of ERα and the PI3K downstream effector Akt induced by icariin, the phosphorylation of IGF-IR, ERα and Akt in MC3T3-E1 cells in response to icariin (0.1 μM) and IGF-1 (100 ng/ml) in the presence or absence of IGF-IR blockers was determined. Pre-treatment of MC3T3-E1 cells with JB-1 (10 μM, a selective IGF-IR antagonist) abolished the stimulatory effects of IGF-1, but not those of icariin, on the phosphorylation of IGF-IR (Figs. 6A and 6B). JB-1 did not significantly alter the effects of either IGF-1 or icariin on phosphorylation of ERα at Ser 167 (also a downstream target of PI3K/Akt pathway) in MC3T3-E1 cells (Fig. 6A and 6C). Pre-treatment of MC3T3-E1 cells with picropodophyllin (PPP) (0.5 μM, IGF-IR kinase inhibitor) for 6 hours completely abolished the phosphorylation of IGF-IR induced by IGF-1 and icariin (Fig. 6D and 6E). Most importantly, blocking of IGF-IR phosphorylation with PPP abolished the effects of IGF-1 and icariin on ERα phosphorylation at Ser 167 (Fig. 6D and 6F) and Akt phosphorylation (Fig. 6G and 6H), suggesting that icariin required the kinase activities of IGF-IR to induce at least both ERα and Akt phosphorylation for osteogenic effects and cell survival. To further confirm if IGF-IR was involved in the direct mediating of the icariin-stimulated osteogenic effects, ALP activities in mature osteoblasts differentiated from BMSCs in response to icariin (0.1 μM) and IGF-1 (100 ng/ml) in the presence or absence of JB-1 or PPP were determined. Pre-treatment of osteoblasts with JB-1 abolished the stimulatory effects of IGF-1, but not those of icariin, on ALP activity (Fig. 6I). Pre-treatment of osteoblasts with PPP completely abolished the ALP activities induced by IGF-1 and icariin (Fig. 6J).

## Discussion

In this report, icariin administrated by using phytoestrogen-free diet at 50, 500 and 3000 ppm (i.e. 2.14, 21.4 and 128.6 mg/kg body weight/day) for three months could ameliorate estrogen-deficiency-induced body weight gain and loss of BMD and micro-architectural properties at all tested bone sites in mature OVX rats. The *in vivo* effects of icariin appeared to be mediated by mimicking the effects of E2 in suppressing the rapid bone turnover induced by estrogen deficiency in OVX rats, as revealed by the inhibitory effects on bone resorption marker (DPD). The effects of icariin were more prominent at the distal femur than at the proximal tibia in OVX rats, as reflected by its effects on cortical porosity as well as microarchitecture properties (BV/TV, Tb/Th, Tb.N, Tb.Sp and SMI). Moreover, its effects on the lumbar vertebra in OVX rats appeared to be dose-dependent with the optimal effect at 500 ppm. *Ex vivo* studies using BMSCs isolated from OVX rats fed with icariin-containing diet further indicated that the effects of icariin on osteoblastogenesis in BMSCs was dose-dependent with stronger effects on osteoblast differentiation (ALP activity) and osteoblast mineralization (Alizarin red and Von Kossa staining) at 50 and 500 ppm while its effects on osteoclastogenesis in BMSCs was dose-independent. These findings were in line with the level of circulating bone marker, with the optimal effects on bone formation marker (PINP) at 500 ppm and with similar effects on bone resorption marker (DPD) at all tested dosages.

Previous studies have indicated that the bone anabolic effects of icariin are ER-dependent (Mok et al., 2010; Song et al., 2013; Wu et al., 2017), and our recent study has shown that icariin is not a ligand of either ERα or ERβ and it activates ERα ligand-independently by phosphorylation via MAPK/ERK and PI3K/Akt dependent pathways in osteoblastic cells (Ho et al., 2018). However, the mechanism by which icariin exerts bone protective effects *in vivo* is far from clear. GO enrichment and KEGG pathway analysis of RNA-Seq data comparing samples from icariin treated rats (500 ppm versus OVX), shows that icariin significantly alters the gene expression involved in cell adhesion, focal adhesion as well as actin cytoskeleton in BMSCs. The actions of icariin in bone cells appear to be similar to those activated by mechanical loading and ligand-independent activation of ERα (Jessop et al., 2001; Windahl et al., 2013) as well as the activation of cell adhesion, focal adhesion and actin cytoskeleton (Jansen et al., 2017) have been reported previously.

Both IGF-IR (Tian et al., 2018) and ER (Jessop et al., 2001; Windahl et al., 2013), as well as their cross-talk (Sunters et al., 2010) are reported to play an important role in

mechanotransduction. Thus, it is of interest to determine if icariin also mimics the effects of mechanical loading in altering IGF-IR and downstream PI3K-Akt signaling pathways in bone tissues. Our RNA-Seq results clearly indicate that icariin alters IGF-1 signaling pathways by inducing IGF-1 mRNA and suppressing IGF-IR and IRS-1 mRNA expression in BMSCs. Moreover, icariin at 500 ppm significantly alters the mRNA expression of subunits of PI3K, nitric oxide synthase 3 (NOS3) and Bcl-2 in BMSCs, indicating that PI3K signaling, the downstream of IGF-1 signaling, are also altered in OVX rats. Using BMSCs and MC3T3-E1 cells, we further show that icariin could rapidly induce physical interactions between IGF-IR and ERα. Subsequent studies on MC3T3-E1 cells show that icariin can rapidly increase IRS-1 expression and IGF-IR phosphorylation within 10 minutes of incubation. Most importantly, blocking IGF-IR with the specific IGF-IR kinase blocker PPP completely abolishes the effect of icariin on the phosphorylations of IGF-IR, ERα at Ser 167 and Akt in MC3T3-E1 cells, confirming the role of IGF-IR-ERα crosstalk and the direct interaction of IGF-IR and Akt activation in mediating the effects of icariin in cells of osteoblastic lineage. Most importantly, PPP can completely abolish the effect of icariin on ALP activity in osteoblasts differentiated from BMSCs, which further confirms the direct effect of IGF-IR activation on mediating the osteogenic effects of icariin.

The present study confirms that icariin could exert tissue-selective estrogen-like effects on bone without inducing any undesirable effects on the uterus. Its bone protective actions appear to be similar to those of raloxifene, a clinically prescribed SERM for treatment of osteoporosis. The dosage of raloxifene (1 mg/kg/day) applied in this study is the effective dosage in a previous animal study (Iwamoto et al., 2005). Both icariin and raloxifene suppressed estrogen deficiency-induced bone turnover and exerted estrogen-like bone protective effects at all tested sites. RNA-seq analysis of BMSCs derived from treated rats revealed that icariin at 500 ppm and raloxifene exert very similar effects on the mRNA expression of IGF-I as well as genes involved in bone formation and PI3K-Akt signaling pathways. A previous *in vitro* study has demonstrated that raloxifene stimulates endothelial nitric oxide synthase (eNOS) via PI3K-Akt signaling pathway in human umbilical vein endothelial cells (Simoncini et al., 2002). Moreover, icariin could improve cortical porosity at the distal femur, suggesting that it might have similar osteogenic effects as E2 in improving overall bone strength in OVX rats. *Ex vivo* studies using BMSCs from

these animals show that icariin appears to exert similar effects as raloxifene on osteoclastogenesis and osteoblastogenesis, but less effect on cortical porosity.

Our previous study (Ho et al., 2018) has indicated that icariin behaves as pathway-selective SERMs to activate ERs by rapid signaling without inducing any classical genomic events. These actions can account for the potent osteogenic effects of icariin and its ability to rapidly activate ERα in a ligand-independent manner. In conclusion, the *in vivo* study characterized the dose-specific osteogenic effects of icariin on bone and the *in vitro* study further increased our understanding of the potential actions of icariin in enhancing IGF-1 signaling pathways in bone tissues, possibly by increasing 1) the expression and phosphorylation of IGF-IR, IRS-1 and the downstream effector Akt in osteoblastic cells and 2) the physical interactions and cross-talk between IGF-IR and ERα. As impairment in IGF-1 signaling is believed to contribute to the age-related loss of osteogenic potential in BMSCs (Chen et al., 2017), the ability of icariin to enhance IGF-1 signaling in osteoblasts would make it a good candidate for managing not only postmenopausal, but also the age-related osteoporosis. A limitation of the present study is the secretion of IGF-1 not been detected. Future study will be needed to demonstrate if icariin can promote new bone growth in OVX model by applying calcein and alizarin red for double labeling new bone formation, evaluate the expression and serum level of IGF-1 and its binding protein IGFBP3 and also characterize the mechanism by which icariin activate IGF-IR as well as to elucidate its effects on cell adhesion and regulation of actin cytoskeleton in osteoblastic cells.

## Funding

This work was supported by the General Research Fund (15103614) and Collaborative Research Fund Equipment Grant (C5012-15E) of Research Grant Council (HKSAR), Hundred Talents Program from Shanghai Municipal Commission of Health and Family Planning (2018BR03), Program of Shanghai Academic Research Leader (19XD1423800) and the Hong Kong Polytechnic University research studentship for Dr. Liping Zhou.

## Acknowledgements

We thank State Key Laboratory of Chinese Medicine and Molecular Pharmacology (Incubation), Shenzhen and Essential Drug Research and Development (2019ZX09201004-003-032) from Ministry of Science and Technology of China for their financial support. We also thank the University Research Facility in Life Sciences at the Hong Kong Polytechnic University for their technical support.

## Author contributions

LZ, CCWP, KYW and SC performed experiments; LZ and CCWP analyzed data, prepared the figures and drafted the manuscript; XD, YZ and MSW designed the study.

## Declaration of competing interest

The authors declare that the research was conducted in the absence of any commercial or financial relationships that could be construed as a potential conflict of interest.

## References


Arnal, J.-F., Metivier, R., Flouriot, G., Hention, D., Adlanmerini, M., Fontaine, C., Gourdy, P., Chambon, P., Katzenellenbogen, B., Katzenellenbogen, J., 2017. Membrane and Nuclear Estrogen Receptor Alpha Actions: From Tissue Specificity to Medical Implications.(Report). Physiological Reviews 97, 1045-1088.

Barrett-Connor, E., Mosca, L., Collins, P., Geiger, M.J., Grady, D., Kornitzer, M., McNabb, M.A., Wenger, N.K., Raloxifene Use for The Heart Trial, I., 2006. Effects of raloxifene on cardiovascular events and breast cancer in postmenopausal women. N Engl J Med 355, 125-137.

Bartell, S.M., Han, L., Kim, H.N., Kim, S.H., Katzenellenbogen, J.A., Katzenellenbogen, B.S., Chambliss, K.L., Shaul, P.W., Roberson, P.K., Weinstein, R.S., Jilka, R.L., Almeida, M., Manolagas, S.C., 2013. Non-nuclear-initiated actions of the estrogen receptor protect cortical bone mass. Mol Endocrinol 27, 649-656.

Britz, H.M., Jokihaara, J., Leppanen, O.V., Jarvinen, T., Cooper, D.M., 2010. 3D visualization and quantification of rat cortical bone porosity using a desktop micro-CT system: a case study in the tibia. J Microsc 240, 32-37.

Chen, C.Y., Tseng, K.Y., Lai, Y.L., Chen, Y.S., Lin, F.H., Lin, S., 2017. Overexpression of Insulin-Like Growth Factor 1 Enhanced the Osteogenic Capability of Aging Bone Marrow Mesenchymal Stem Cells. Theranostics 7, 1598-1611.

Chen, J.R., Lazarenko, O.P., Wu, X., Kang, J., Blackburn, M.L., Shankar, K., Badger, T.M., Ronis, M.J., 2010. Dietary-induced serum phenolic acids promote bone growth via p38 MAPK/beta-catenin canonical Wnt signaling. J Bone Miner Res 25, 2399-2411.

Cooper, D.M., Kawalilak, C.E., Harrison, K., Johnston, B.D., Johnston, J.D., 2016. Cortical Bone Porosity: What Is It, Why Is It Important, and How Can We Detect It? Curr Osteoporos Rep 14, 187-198.

Glurich, I., Chyou, P.H., Engel, J.M., Cross, D.S., Onitilo, A.A., 2013. Tamoxifen-induced venothromboembolic events: exploring validation of putative genetic association. Clin Med Res 11, 16-25.

Gustafsson, K.L., Farman, H., Henning, P., Lionikaite, V., Moverare-Skrtic, S., Wu, J., Ryberg, H., Koskela, A., Gustafsson, J.A., Tuukkanen, J., Levin, E.R., Ohlsson, C., Lagerquist, M.K., 2016. The role of membrane ERalpha signaling in bone and other major estrogen responsive tissues. Sci Rep 6, 29473.

Ho, M.-X., Poon, C.C.W., Wong, K.-C., Qiu, Z.-C., Wong, M.-S., 2018. Icariin, but Not Genistein, Exerts Osteogenic and Anti-apoptotic Effects in Osteoblastic Cells by Selective Activation of Non-genomic ERα Signaling. Frontiers in Pharmacology 9, 474.

Iwamoto, J., Yeh, J.K., Schmidt, A., Rowley, E., Stanfield, L., Takeda, T., Sato, M., 2005. Raloxifene and vitamin K2 combine to improve the femoral neck strength of ovariectomized rats. Calcif Tissue Int 77, 119-126.

Jansen, K.A., Atherton, P., Ballestrem, C., 2017. Mechanotransduction at the cell-matrix interface. Semin Cell Dev Biol 71, 75-83.

Jessop, H.L., Sjoberg, M., Cheng, M.Z., Zaman, G., Wheeler-Jones, C.P., Lanyon, L.E., 2001. Mechanical strain and estrogen activate estrogen receptor alpha in bone cells. J Bone Miner Res 16, 1045-1055.

Kanehisa, M., Araki, M., Goto, S., Hattori, M., Hirakawa, M., Itoh, M., Katayama, T., Kawashima, S., Okuda, S., Tokimatsu, T., Yamanishi, Y., 2008. KEGG for linking genomes to life and the environment. Nucleic Acids Res 36, D480-484.

Kato, S., Endoh, H., Masuhiro, Y., Kitamoto, T., Uchiyama, S., Sasaki, H., Masushige, S., Gotoh, Y., Nishida, E., Kawashima, H., Metzger, D., Chambon, P., 1995. Activation of the Estrogen Receptor Through Phosphorylation by Mitogen-Activated Protein Kinase. Science 270, 1491-1494.
Khalid, A.B., Krum, S.A., 2016. Estrogen receptors alpha and beta in bone. Bone 87, 130-135.
Khosla, S., Amin, S., Orwoll, E., 2008. Osteoporosis in men. Endocr Rev 29, 441-464.
Khosla, S., Monroe, D.G., 2018. Regulation of Bone Metabolism by Sex Steroids. Cold Spring Harbor perspectives in medicine 8.
Li, N., Lee, W.Y., Lin, S.E., Ni, M., Zhang, T., Huang, X.R., Lan, H.Y., Li, G., 2014. Partial loss of Smad7 function impairs bone remodeling, osteogenesis and enhances osteoclastogenesis in mice. Bone 67, 46-55.
Manolagas, S.C., O'Brien, C.A., Almeida, M., 2013. The role of estrogen and androgen receptors in bone health and disease. Nat Rev Endocrinol 9, 699-712.
Marino, S., Logan, J.G., Mellis, D., Capulli, M., 2014. Generation and culture of osteoclasts. Bonekey Rep 3, 570.
Mirkin, S., Komm, B.S., 2013. Tissue-selective estrogen complexes for postmenopausal women. Maturitas 76, 213-220.
Mok, S.K., Chen, W.F., Lai, W.P., Leung, P.C., Wang, X.L., Yao, X.S., Wong, M.S., 2010. Icariin protects against bone loss induced by oestrogen deficiency and activates oestrogen receptor-dependent osteoblastic functions in UMR 106 cells. Br J Pharmacol 159, 939-949.
Nyirjesy, I., 2003. Breast cancer and hormone-replacement therapy: the Million Women Study. Lancet 362, 1330; author reply 1330-1331.
Riggs, B.L., Khosla, S., Melton, L.J., 3rd, 2002. Sex steroids and the construction and conservation of the adult skeleton. Endocr Rev 23, 279-302.
Rossouw, J.E., Anderson, G.L., Prentice, R.L., LaCroix, A.Z., Kooperberg, C., Stefanick, M.L., Jackson, R.D., Beresford, S.A., Howard, B.V., Johnson, K.C., Kotchen, J.M., Ockene, J., Writing Group for the Women's Health Initiative, I., 2002. Risks and benefits of estrogen plus progestin in healthy postmenopausal women: principal results From the Women's Health Initiative randomized controlled trial. JAMA 288, 321-333.
Simoncini, T., Genazzani, A.R., Liao, J.K., 2002. Nongenomic mechanisms of endothelial nitric oxide synthase activation by the selective estrogen receptor modulator raloxifene. Circulation 105, 1368-1373.
Song, L., Zhao, J., Zhang, X., Li, H., Zhou, Y., 2013. Icariin induces osteoblast proliferation, differentiation and mineralization through estrogen receptor-mediated ERK and JNK signal activation. European journal of pharmacology 714, 15-22.
Sunters, A., Armstrong, V.J., Zaman, G., Kypta, R.M., Kawano, Y., Lanyon, L.E., Price, J.S., 2010. Mechano-transduction in osteoblastic cells involves strain-regulated estrogen receptor alpha-mediated control of insulin-like growth factor (IGF) I receptor sensitivity to Ambient IGF, leading to phosphatidylinositol 3-kinase/AKT-dependent Wnt/LRP5 receptor-independent activation of beta-catenin signaling. J Biol Chem 285, 8743-8758.
Taylor, S.E., Shah, M., Orriss, I.R., 2014. Generation of rodent and human osteoblasts. Bonekey Rep 3, 585.
Tian, F., Wang, Y., Bikle, D.D., 2018. IGF-1 signaling mediated cell-specific skeletal mechano-transduction. J Orthop Res 36, 576-583.
Wang, Z., Wang, D., Yang, D., Zhen, W., Zhang, J., Peng, S., 2018. The effect of icariin on bone metabolism and its potential clinical application. Osteoporos Int 29, 535-544.

Wei, Q., Zhang, J., Hong, G., Chen, Z., Deng, W., He, W., Hui Chen, M., 2016. Icariin promotes osteogenic differentiation of rat bone marrow stromal cells by activating the ERα-Wnt/β-catenin signaling pathway.

Windahl, S.H., Saxon, L., Borjesson, A.E., Lagerquist, M.K., Frenkel, B., Henning, P., Lerner, U.H., Galea, G.L., Meakin, L.B., Engdahl, C., Sjogren, K., Antal, M.C., Krust, A., Chambon, P., Lanyon, L.E., Price, J.S., Ohlsson, C., 2013. Estrogen receptor-alpha is required for the osteogenic response to mechanical loading in a ligand-independent manner involving its activation function 1 but not 2. J Bone Miner Res 28, 291-301.

Wu, Z., Ou, L., Wang, C., Yang, L., Wang, P., Liu, H., Xiong, Y., Sun, K., Zhang, R., Zhu, X., 2017. Icaritin induces MC3T3-E1 subclone14 cell differentiation through estrogen receptor-mediated ERK1/2 and p38 signaling activation. Biomedicine & pharmacotherapy = Biomedecine & pharmacotherapie 94, 1-9.

Xiao, H.H., Fung, C.Y., Mok, S.K., Wong, K.C., Ho, M.X., Wang, X.L., Yao, X.S., Wong, M.S., 2014. Flavonoids from Herba epimedii selectively activate estrogen receptor alpha (ERalpha) and stimulate ER-dependent osteoblastic functions in UMR-106 cells. J Steroid Biochem Mol Biol 143, 141-151.

Ye, J., Fang, L., Zheng, H., Zhang, Y., Chen, J., Zhang, Z., Wang, J., Li, S., Li, R., Bolund, L., Wang, J., 2006. WEGO: a web tool for plotting GO annotations. Nucleic Acids Res 34, W293-297.

Zhang, G., Qin, L., Shi, Y., 2007. Epimedium-derived phytoestrogen flavonoids exert beneficial effect on preventing bone loss in late postmenopausal women: a 24-month randomized, double-blind and placebo-controlled trial. J Bone Miner Res 22, 1072-1079.

Zhou, L.P., Wong, K.Y., Yeung, H.T., Dong, X.L., Xiao, H.H., Gong, A.G., Tsim, K.W., Wong, M.S., 2018. Bone Protective Effects of Danggui Buxue Tang Alone and in Combination With Tamoxifen or Raloxifene in vivo and in vitro. Front Pharmacol 9, 779.

## Figure legends

**Fig. 1.** The osteogenic effects of icariin on bone turnover markers (serum PINP and urinary DPD), BMD and cortical bone porosity in OVX rats. Serum level of PINP (A) and urinary level DPD (B) were measured by ELISA kits. BMD analysis by μ-CT (C) on the trabecular bone of the distal femur, proximal tibia and lumbar vertebra at L4 and cortical bone porosity analysis by μ-CT (D) on the cortical bone of femur and tibia in OVX rats with long-term treatments with icariin for 3 months were evaluated. The values represent the means ± SEM determined by using (A-C) one-way ANOVA followed by Tukey's *post hoc* test, $^{***}p<0.001$ versus sham; $^{\wedge}p<0.05$, $^{\wedge\wedge}p<0.01$ and $^{\wedge\wedge\wedge}p<0.001$ versus OVX (n=6 – 10/group); (D) one-way ANOVA followed by Tukey's *post hoc* test, $^{**}p<0.01$ and $^{***}p<0.001$ versus sham and $^{\wedge}p<0.05$, $^{\wedge\wedge}p<0.01$ and $^{\wedge\wedge\wedge}p<0.001$ versus OVX (n=10-12/group).

**Fig. 2.** The osteogenic effects of icariin on osteogenic differentiation (ALP activity) and mineralization (formation of calcium deposits and phosphate mineralized nodules) in BMSCs isolated from OVX rats. Representative images of ALP staining (A)(i) in BMSCs cultured in osteogenic medium of each group on day 10 and the quantification (A)(ii) of the number of red colonies of osteoblasts reflecting the ALP activity. Representative images of Alizarin red staining (B)(i) and Von Kossa staining (C) in BMSCs cultured in osteogenic medium of each group on day 25. The osteoblasts with calcium phosphate mineralized nodules were stained in brownish black . The graph (B)(ii) shows quantification of calcium deposits in osteoblasts using colorimetric methods. Representative images of TRAP staining (D)(i) in osteoclasts cultured in osteoclastogenic medium of each group on day 13 (scale bar: 50 μm). TRAPase-positive (shown as purple) with multinucleated osteoclasts and the quantification (D)(ii) of the number of multinucleated osteoclasts are shown. The values represent the means ± SEM determined by using one-way ANOVA followed by Tukey's *post hoc* test, $^{*}p<0.05$ and $^{***}p<0.001$ versus sham; $^{\wedge}p<0.05$, $^{\wedge\wedge}p<0.01$ and $^{\wedge\wedge\wedge}p<0.001$ versus OVX (n=6/group).

**Fig. 3.** RNA sequencing analysis of the long-term icariin treatment of BMSCs isolated from OVX rats. The mRNA heatmap (A) displaying hierarchical cluster of the expression levels of differentially expressed genes (DEGs) between sham vs. OVX, OVX vs. E2, OVX vs. Raloxifene, OVX vs. icariin at 50 ppm (ICA50), 500 ppm (ICA500) or 3000 ppm (ICA3000).

Hierarchical cluster analysis was conducted for DEGs using log2 ratio and $p<0.05$. The scatter plot (B, Left panel) and the volcano plot (B, Right panel) of significantly differentially expressed genes (DEGs) between OVX vs. icariin at 500 ppm. Dots in red mean significant DEGs which passed screening threshold and black dots are non-significant DEGs. Gene ontology (GO) functional analysis (C) of DEGs in the comparison between OVX and icariin at 500 ppm. The GO enrichment analysis grouped these DEGs into functional groups. The Y axis represents GO terms. All GO terms are grouped into 3 ontologies: blue is for biological process, green is for cellular component and red is for molecular function. Statistics of KEGG (Kyoto Encyclopedia of Genes and Genomes) pathway enrichment of DEGs (D) in the comparison between OVX and icariin at 500 ppm. KEGG pathway analysis of the top 20 KEGG enriched gene pathway-related diseases. These differentially expressed genes were grouped into gene pathways using the pathway enrichment analysis with the KEGG database and KOBAS software. Q-value is corrected p-value ranging from 0-1 and smaller Q-value means greater intensiveness. Fragments per kilobase of transcript per million mapped reads (FPKM) values were used to calculate gene expression in RNA-seq and to normalize the expression level as fold change compared with sham group.

**Fig. 4.** The acute effect of icariin on ERα and IGF-IR cross-talk in rat BMSCs and osteoblastic cells. Representative confocal microscopic images (A)(a-d) displaying icariin-induced colocalization of IGF-IR and ERα in response to the treatments of IGF-I (100 ng/ml), E2 (10 nM) or icariin (0.1 μM) for 10 min in rat BMSCs. The representative images were captured at mid-plane of cells and visualized using a confocal laser scanning microscope (magnification: 600x and scale bar: 10 μm). Representative 3-D fluorescence images (A)(e-h) of icariin-induced colocalization of IGF-IR and ERα in response to the treatments (scale bar: 10 μm). Hoechst counter-staining (blue) was applied for determination of single cell. The quantification (B) of total fluorescent intensities of Alexa488-IGF-IR positive cells (shown in green) and Alexa594-ERα positive cells (shown in red) and the quantification (C) of co-localization of IGF-IR and ERα. The representative blots of co-immunoprecipitation (D) of IRS1, IGF-IR and ERα in rat BMSCs in response to the treatments of Des1,3-IGF-1 (100 ng/ml), IGF-1 (100 ng/ml) or icariin (0.1 μM) for 10 min. The values represent the means ± SEM determined by using one-way

ANOVA followed by Tukey's *post hoc* test, $^{*}p<0.05$, $^{**}p<0.01$ and $^{***}p<0.001$ versus control (n=5/group).

**Fig. 5.** The dose- and time-dependent effects of icariin on the protein expressions of IRS1 and IRS2 and phosphorylation of IGF-IR in MC3T3-E1 cells. Representative immunoblots (A) show the protein expressions of IRS1, IRS2, phosphorylated IGF-IR and total IGF-IR and the quantification of relative ratio of expressions of IRS1 (B), IRS2 (C) and phosphorylated IGF-IR (D) in response to the treatments of IGF-I (100 ng/ml), E2 (10 nM), icariin (10 nM, 0.1 μM and 1 μM) or vehicle (control) in MC3T3-E1 cells for 10 min. Representative immunoblots (E) show the protein expressions of phosphorylated IRS1 at tyrosine 612 and total IRS1 and the quantification (F) of relative ratio of the expressions in MC3T3-E1 cells for 0-30 min in response to the treatments of IGF-I (100 ng/ml), E2 (10 nM) or icariin (0.1 μM). The values represent the means ± SEM determined by using one-way ANOVA followed by Tukey's *post hoc* test, $^{*}P<0.05$, $^{**}P<0.01$ and $^{***}P<0.001$ versus control (n=5).

**Fig. 6.** Blocking of IGF-IR with IGF-IR kinase inhibitor picropodophyllin (PPP) completely abolished the stimulatory effects of icariin on phosphorylation of both IGF-IR and ERα in MC3T3-E1 cells, but not with IGF-1 antagonist JB-1. Representative immunoblots for the inhibitory effects of JB-1 (A) on the phosphorylation of IGF-IR and ERα at serine 167 and the quantification of relative ratio of expressions of phosphorylated IGF-IR (B) and phosphorylated ERα at serine 167 (C) in the presence of JB-1. Representative immunoblots for the inhibitory effects of PPP on the phosphorylation of IGF-IR and ERα at serine 167 (D) and on the phosphorylation of Akt (G) the quantification of relative ratio of expressions of phosphorylated IGF-IR (E), phosphorylated ERα at serine 167 (F) and phosphorylated Akt (H) in the presence of PPP. PPP completely abolished the stimulatory effects of IGF-1 and icariin on alkaline phosphatase (ALP) activities in BMSCs (J), but not with IGF-1 antagonist JB-1 (I). The values represent the means ± SEM determined by using one-way ANOVA followed by Tukey's *post hoc* test, $^{*}P<0.05$ and $^{***}P<0.001$; $^{\#}P<0.05$, $^{\#\#}P<0.01$ and $^{\#\#\#}P<0.001$ versus control (n=5).

**Table 1.** The long-term effects of icariin on body weight, uterus index and biochemical parameters of OVX rats. The values represent the means ± SEM determined by using one-way

ANOVA followed by Tukey's *post hoc* test, $^{**}p<0.05$ and $^{***}p<0.001$ versus sham; $^{\wedge\wedge}p<0.01$ and $^{\wedge\wedge\wedge}p<0.001$ versus OVX (n=10-12/group).

**Table 2.** List of differential expressed genes (DEGs) in treatment groups of rat BMSCs related to osteogenesis.

**Supplementary Figure 1.** The osteogenic effects of icariin on the micro-structure of trabecular bone at the distal femur, proximal tibia and lumbar vertebra in OVX rats. Representative micro-computed tomography (μ-CT) images of the trabecular bone of the distal femur (A), proximal tibia (B) and lumbar vertebra (C) in OVX rats treated with diets containing icariin at 50, 500, 3000 ppm or positive control (E2, 1 mg/kg; raloxifene, 1 mg/kg) or the control diet for 3 months.

**Supplementary Figure 2.** The osteogenic effects of icariin on osteogenic differentiation (ALP activity) and mineralization (formation of calcium deposits and phosphate mineralized nodules) in BMSCs isolated from OVX rats. Representative images of ALP staining A(i) in BMSCs cultured in osteogenic medium of each group on day 25 (Magnification: 400x). Representative images of Alizarin red staining B(i) in BMSCs cultured in osteogenic medium of each group on day 10 (Magnification: 400x). Representative images of Von Kossa staining (C) in BMSCs cultured in osteogenic medium of each group on day 10 (Magnification: 400x).

**Supplementary Figure 3.** Verification of DEGs (IGF-IR (A), IRS1 (B) and IRS2 (C)) via quantitative real-time polymerase chain reaction (qPCR). In qPCR, GAPDH was used as a housekeeping gene. The values represent the means ± SEM determined by using one-way ANOVA followed by Tukey's *post hoc* test, $^{*}p<0.05$, $^{**}p<0.01$ and $^{***}p<0.001$ versus sham; $^{\wedge\wedge}p<0.05$, $^{\wedge\wedge}p<0.01$ and $^{\wedge\wedge\wedge}p<0.001$ versus OVX (n=6-8/group).

**Supplementary Table 1.** The osteogenic effects of icariin on (A) the trabecular bone and (B) cortical bone properties at the distal femur, proximal tibia and lumbar vertebra in OVX rats. Trabecular bone properties including bone volume fraction (BV/TV), trabecular bone number (Tb.N, $mm^{-1}$), trabecular bone thickness (Tb.Th, mm), trabecular bone separation (Tb.Sp, mm), connective density (Conn.D, $1/mm^3$), structure model index (SMI) and cortical bone properties including bone volume fraction (BV/TV) and bone mineral density (BMD; $mg/cm^3$) were evaluated by μ-CT. The values represent the means ± SEM determined by using one-way

ANOVA $P<0.0001$ followed by Tukey's *post hoc* test, $^{**}p<0.01$ and $^{***}p<0.001$ versus sham and $^{\wedge}p<0.05$, $^{\wedge\wedge}p<0.01$ and $^{\wedge\wedge\wedge}p<0.001$ versus OVX (n=10-12/group).

**Supplementary Table 2.** Summary of statistics and quality control information of RNA sequencing data for each sample of BMSCs isolated from OVX rats after treatments.

## Tables

**Table 1. The long-term effects of icariin on body weight, uterus index and biochemical parameters in OVX rats.**

| | Sham | OVX | E2 | Raloxifene | ICA-50 | ICA-500 | ICA-3000 |
|---|---|---|---|---|---|---|---|
| Change of body weight (*percentage to the baseline*) | 36.9±3.9 | 54.2±4.1$^{**}$ | 4.3±1.9$^{\wedge\wedge\wedge}$ | 14.1±2.8$^{\wedge\wedge\wedge}$ | 32.1±2.7$^{\wedge\wedge\wedge}$ | 29.7±3.4$^{\wedge\wedge\wedge}$ | 30.0±2.5$^{\wedge\wedge\wedge}$ |
| Uterus index (*mg/g*) | 1.68±0.08 | 0.28±0.03$^{***}$ | 1.24±0.05$^{\wedge\wedge\wedge}$ | 0.48±0.03$^{\wedge\wedge}$ | 0.28±0.02 | 0.27±0.02 | 0.25±0.01 |
| Serum Ca (*mg/L*) | 103.6±1.7 | 99.1±0.8 | 100.3±0.8 | 96.8±0.4 | 96.5±1.0 | 96.3±0.8 | 98.6±1.7 |
| Serum P (*mg/L*) | 47.3±1.9 | 49.7±1.3 | 50.4±1.6 | 47.9±1.4 | 51.9±2.7 | 51.1±1.6 | 51.7±2.6 |
| Urinary Ca/Cr (*mg/mg*) | 0.11±0.007 | 0.10±0.01 | 0.11±0.007 | 0.11±0.01 | 0.12±0.006 | 0.11±0.01 | 0.12±0.003 |
| Urinary P/Cr (*mg/mg*) | 0.41±0.04 | 0.41±0.02 | 0.42±0.03 | 0.42±0.04 | 0.39±0.06 | 0.40±0.03 | 0.41±0.04 |

**Table 2. List of differential genes in treatment groups of rat BMSCs related to osteogenesis.**

| Related pathway | Gene ID | Gene name (gene symbol) | Fold change | | | | | |
|---|---|---|---|---|---|---|---|---|
| | | | OVX vs. Sham | OVX vs. E2 | OVX vs. Raloxifene | OVX vs. ICA-50 ppm | OVX vs. ICA-500 ppm | OVX vs. ICA-3000 ppm |
| Bone formation markers | 367218 | Runt-related transcription factor 2 (Runx2) | **2.14*** (p<0.001)** | 1.87 | **2.38*** (p<0.001)** | **2.00*** (p<0.001)** | **2.78*** (p<0.001)** | 1.38 |
| | 25295 | Osteocalcin / bone gamma-carboxyglutamate protein (Bglap) | 1.07 | **4.31* (p<0.05)** | **84.8*** (p<0.001)** | **8.67*** (p<0.001)** | **20.70*** (p<0.001)** | **16.15*** (p<0.001)** |
| IGF-1 signaling pathway | 24482 | Insulin-like growth factor 1 (Igf1) | 0.73 | **3.26*** (p<0.001)** | **4.59*** (p<0.001)** | 1.63 | **3.08*** (p<0.001)** | **2.61*** (p<0.001)** |
| | 25718 | Insulin-like growth factor 1 receptor (Igf1r) | 0.54 | 0.66 | 0.51 | **0.47*** (p<0.001)** | **0.45*** (p<0.001)** | 0.58 |
| | 25467 | Insulin receptor substrate 1 (Irs1) | 0.79 | **0.36*** (p<0.001)** | 0.50 | 0.89 | 1.12 | **0.46*** (p<0.001)** |
| PI3K-Akt signaling pathway | 116720 | Phosphatidylinositol-4-phosphate 3-kinase, catalytic subunit type 2 gamma (Pik3c2g) | 1.00 | 0.50 | **3.50* (p<0.05)** | 0.50 | **2.00* (p<0.05)** | 0.50 |
| | 497931 | Phosphoinositide-3-kinase, regulatory subunit 5 (Pik3r5) | 0.71 | 0.53 | **0.21*** (p<0.001)** | 0.55 | **0.33*** (p<0.001)** | 0.80 |
| | 24600 | Nitric oxide synthase 3 (Nos3) | 0.95 | 1.51 | **4.21*** (p<0.001)** | **2.70*** (p<0.001)** | **2.35** (p<0.01)** | 0.81 |
| | 24224 | BCL2, apoptosis regulator (Bcl2) | **2.79* (p<0.05)** | 0.97 | 1.49 | 1.46 | **2.43* (p<0.05)** | 1.82 |

0.5< down-regulated; up-regulated >2

Figure 1

A

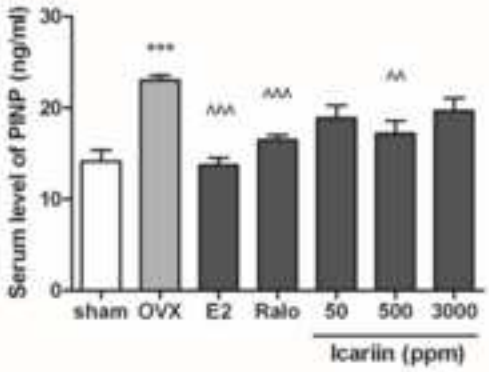


Figure 1

B

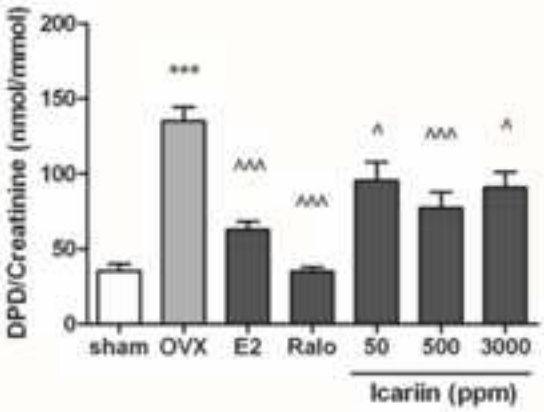


Figure 1

C

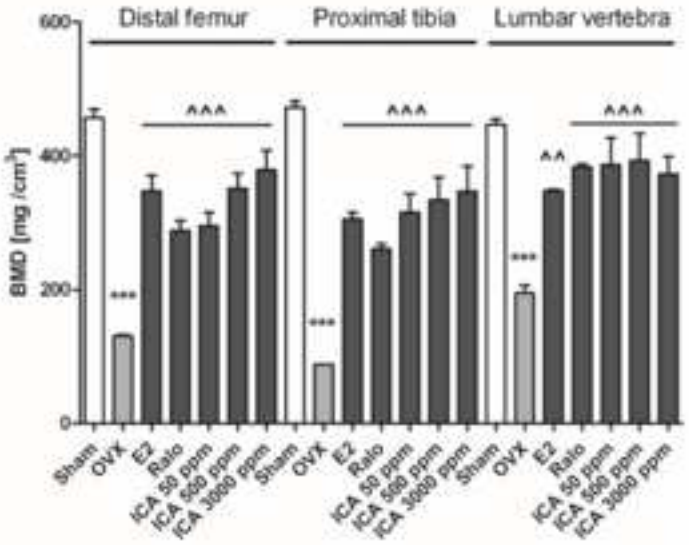


Figure 1

D

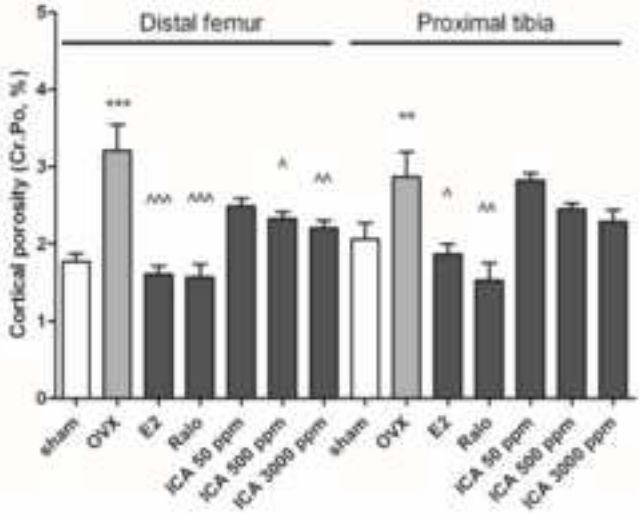

**Figure 2A and 2B**

Figure 2

A(i)

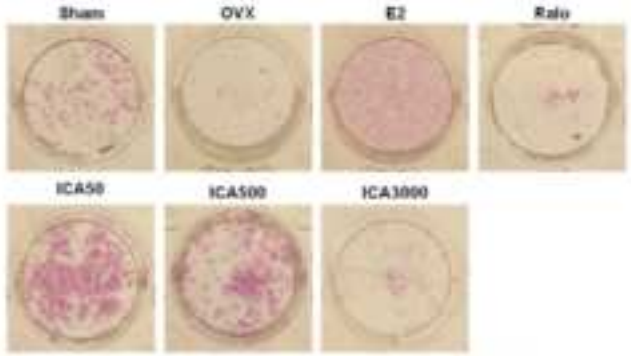


Figure 2

A(ii)

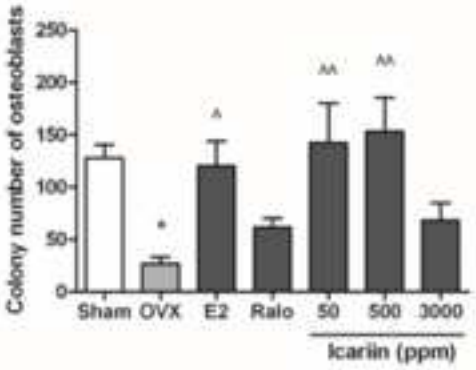


Figure 2

B(i)

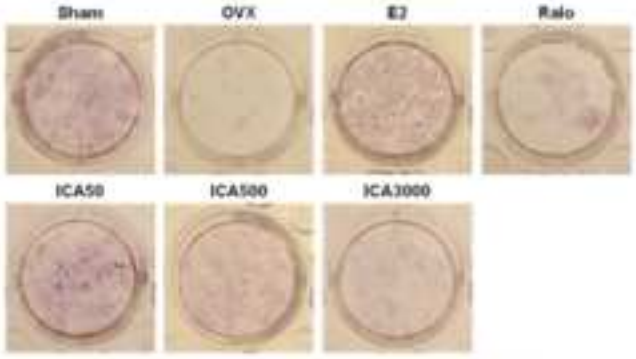


Figure 2

B(ii)

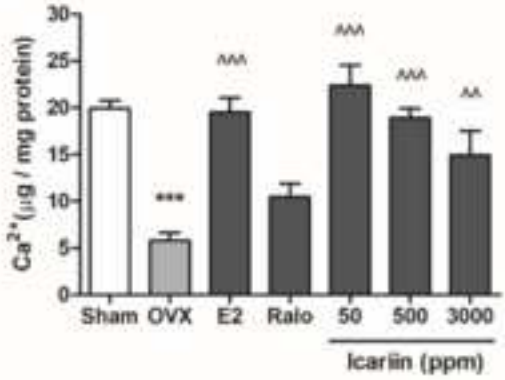

**Figure 2C and 2D(i)**

## Figure 2

### C

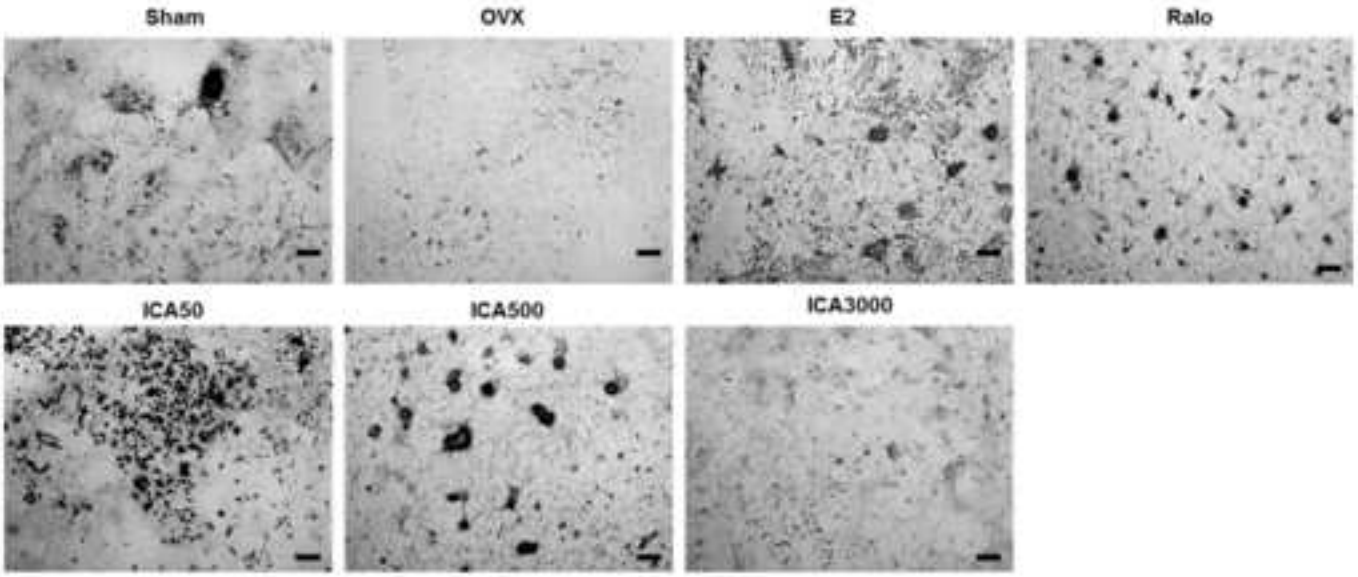


## Figure 2

### D(i)

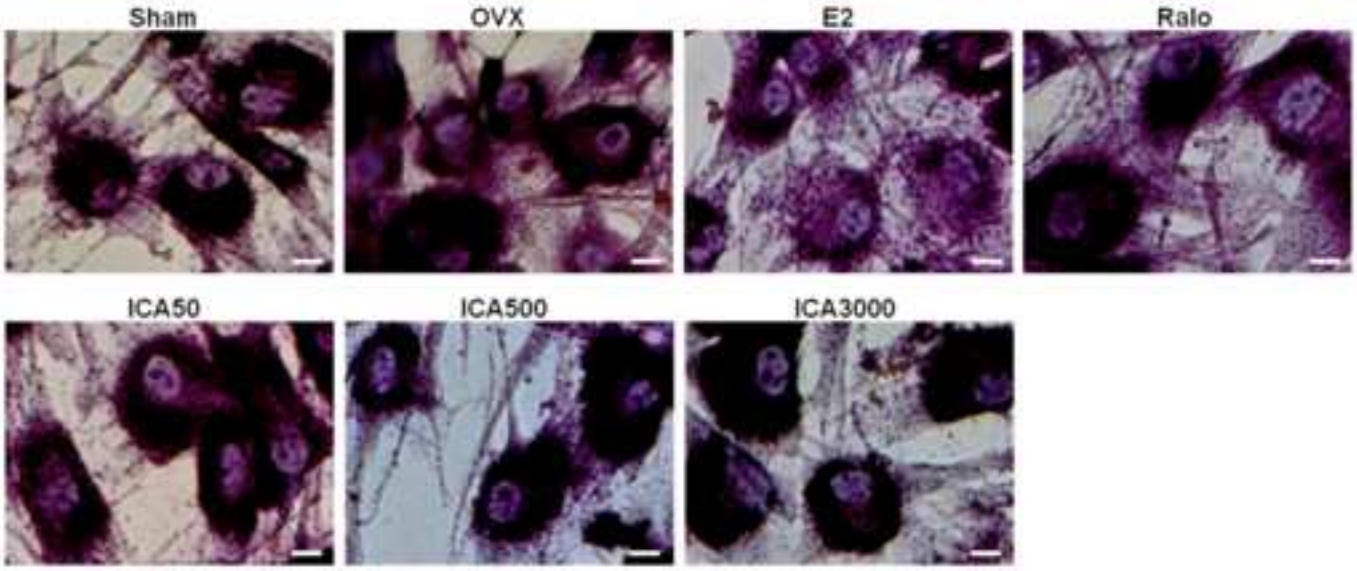

Figure 2D(ii)

Figure 2

D(ii)

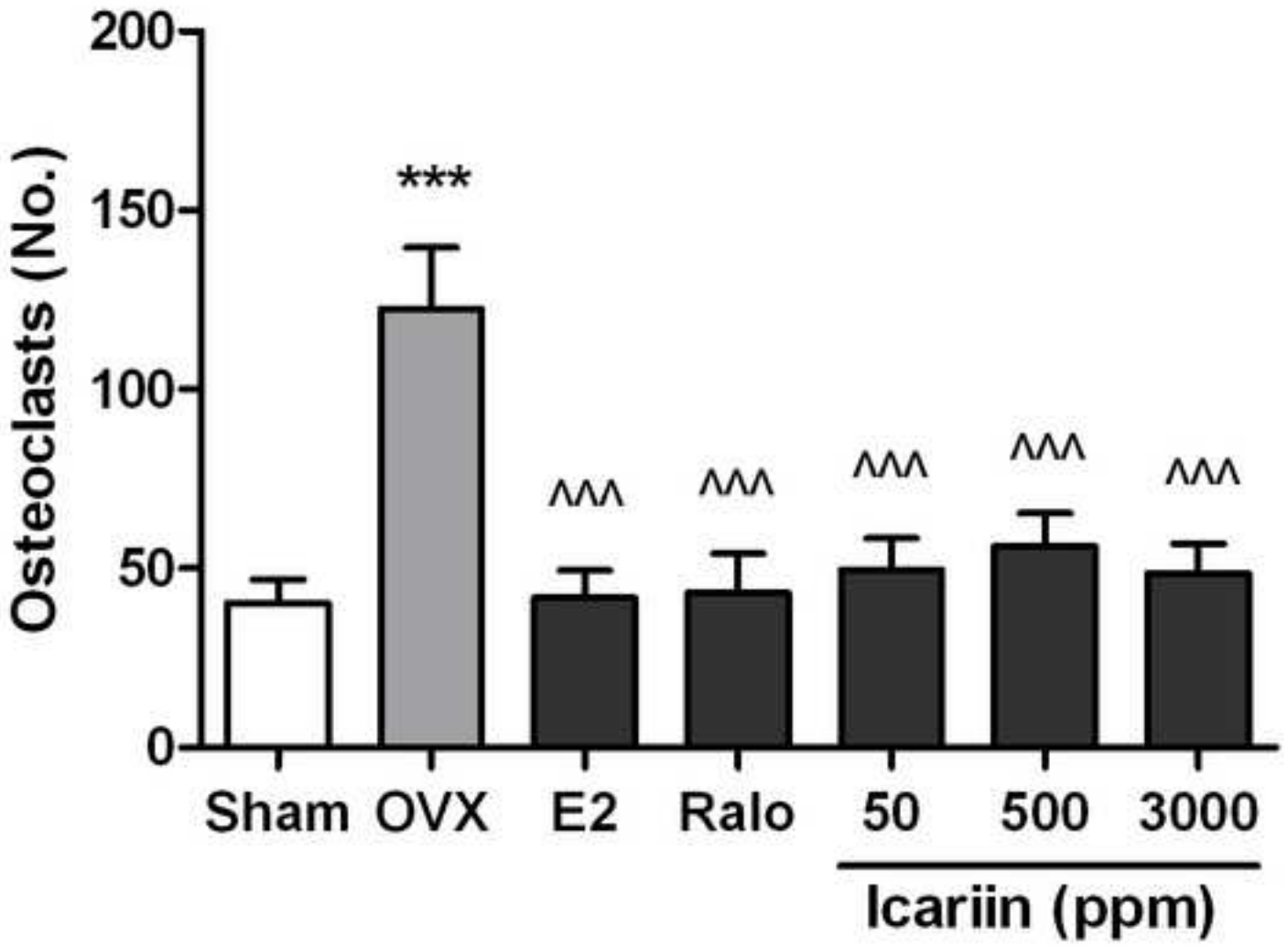

**Figure 3A and 3B**

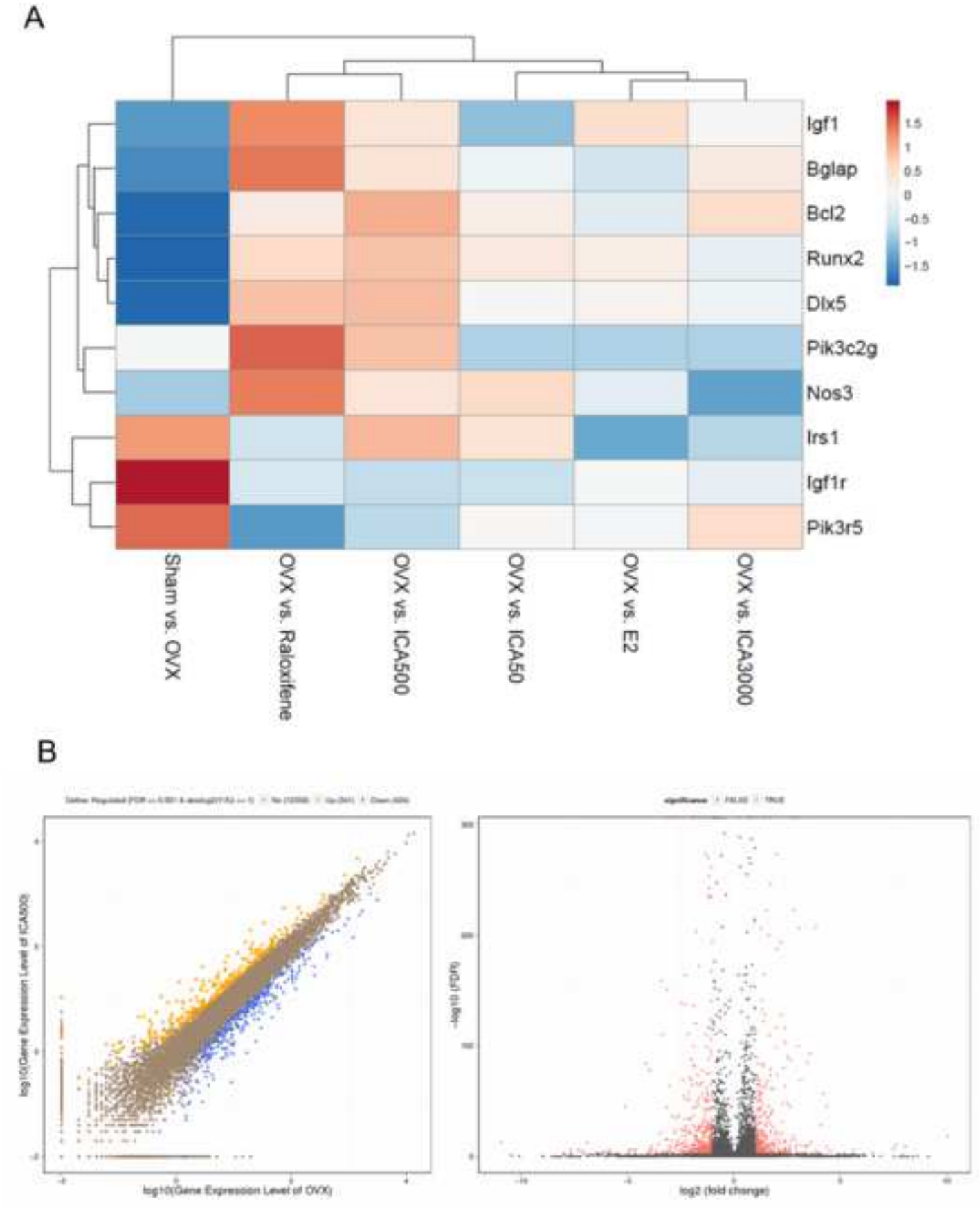

Figure 3C

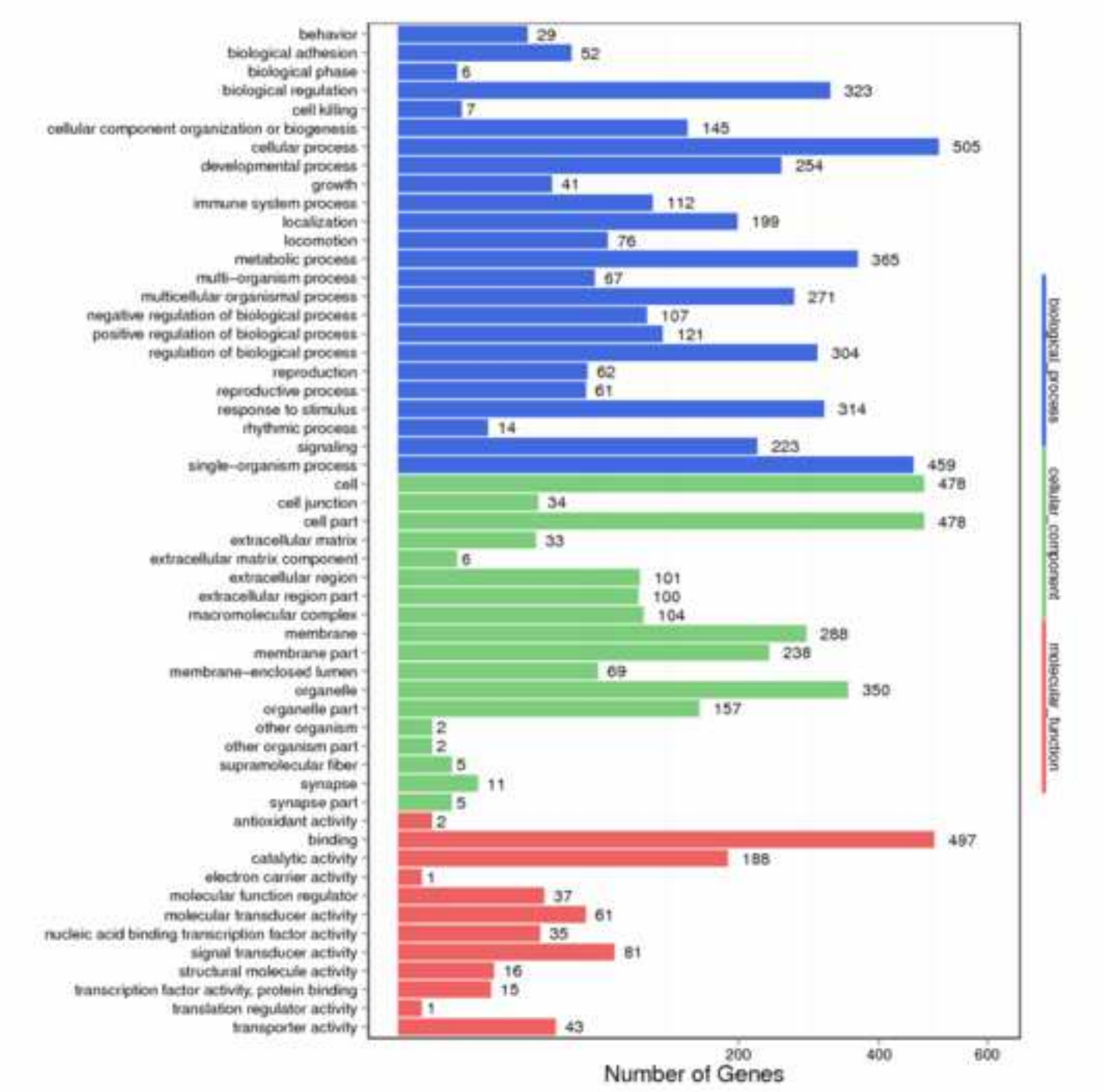
behavior 29
biological adhesion 52
biological phase 6
biological regulation 323
cell killing 7
cellular component organization or biogenesis 145
cellular process 505
developmental process 254
growth 41
immune system process 112
localization 199
locomotion 76
metabolic process 365
multi−organism process 67
multicellular organismal process 271
negative regulation of biological process 107
positive regulation of biological process 121
regulation of biological process 304
reproduction 62
reproductive process 61
response to stimulus 314
rhythmic process 14
signaling 223
single−organism process 459
cell 478
cell junction 34
cell part 478
extracellular matrix 33
extracellular matrix component 6
extracellular region 101
extracellular region part 100
macromolecular complex 104
membrane 288
membrane part 238
membrane−enclosed lumen 69
organelle 350
organelle part 157
other organism 2
other organism part 2
supramolecular fiber 5
synapse 11
synapse part 5
antioxidant activity 2
binding 497
catalytic activity 188
electron carrier activity 1
molecular function regulator 37
molecular transducer activity 61
nucleic acid binding transcription factor activity 35
signal transducer activity 81
structural molecule activity 16
transcription factor activity, protein binding 15
translation regulator activity 1
transporter activity 43
200
400
600
Number of Genes
biological_process
cellular_component
molecular_function

Figure 3D

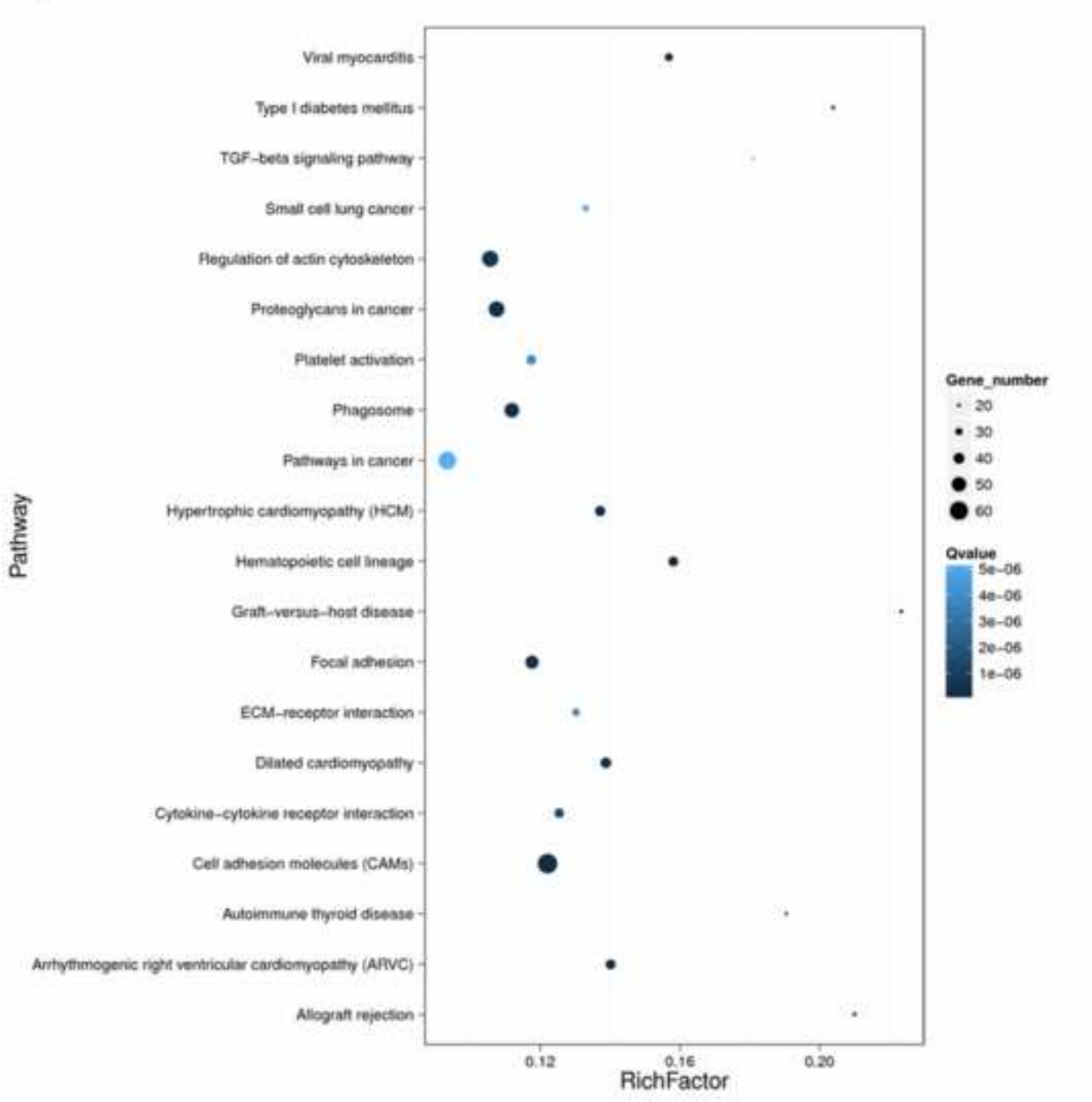
Figure 3D
Viral myocarditis
Type I diabetes mellitus
TGF-beta signaling pathway
Small cell lung cancer
Regulation of actin cytoskeleton
Proteoglycans in cancer
Platelet activation
Phagosome
Pathways in cancer
Hypertrophic cardiomyopathy (HCM)
Hematopoietic cell lineage
Graft-versus-host disease
Focal adhesion
ECM-receptor interaction
Dilated cardiomyopathy
Cytokine-cytokine receptor interaction
Cell adhesion molecules (CAMs)
Autoimmune thyroid disease
Arrhythmogenic right ventricular cardiomyopathy (ARVC)
Allograft rejection
Pathway
0.12
0.16
0.20
RichFactor
Gene_number
20
30
40
50
60
Qvalue
5e-06
4e-06
3e-06
2e-06
1e-06

**Figure 4**

Figure 4

A

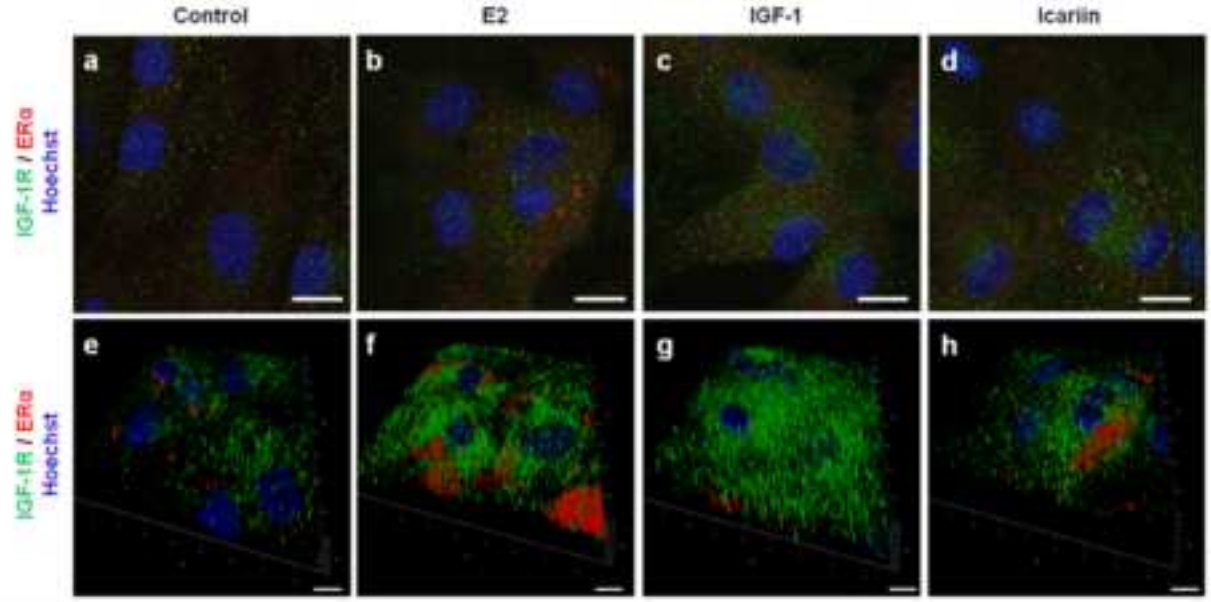


Figure 4

B

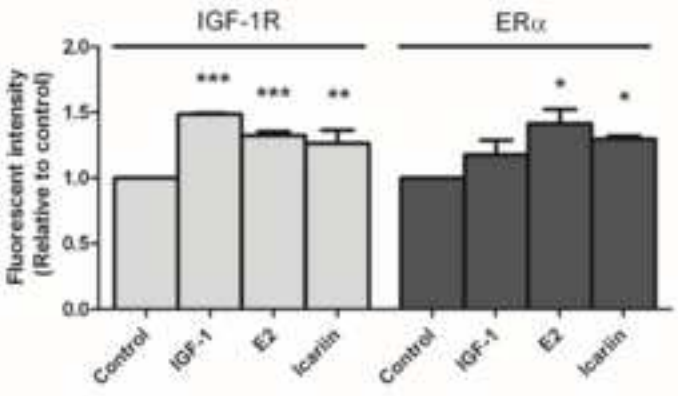


Figure 4

C

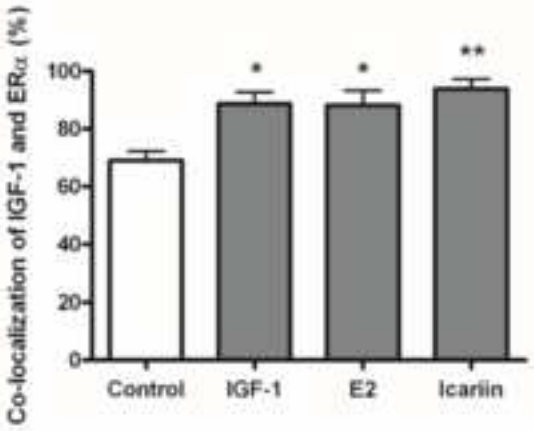


Figure 4

D

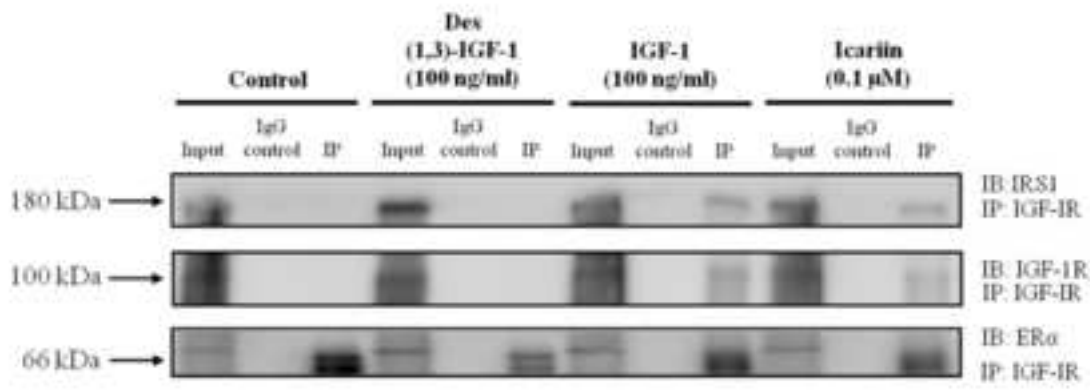

**Figure 5**

Figure 5

A

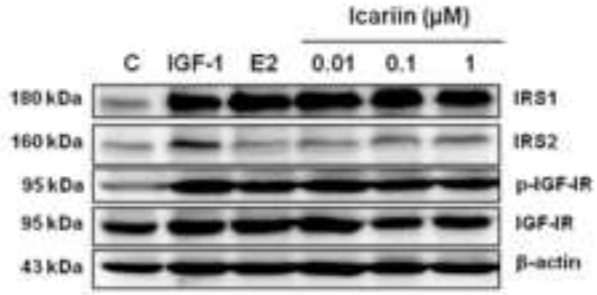


Figure 5

B

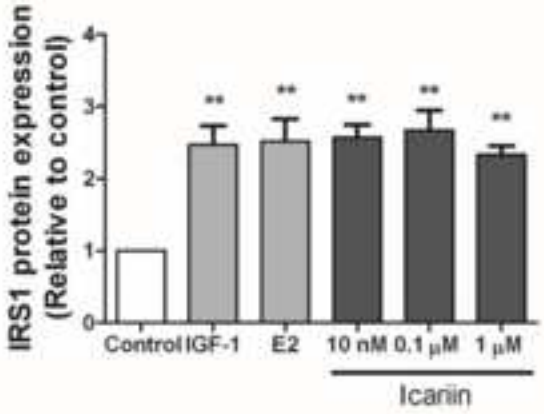


Figure 5

C

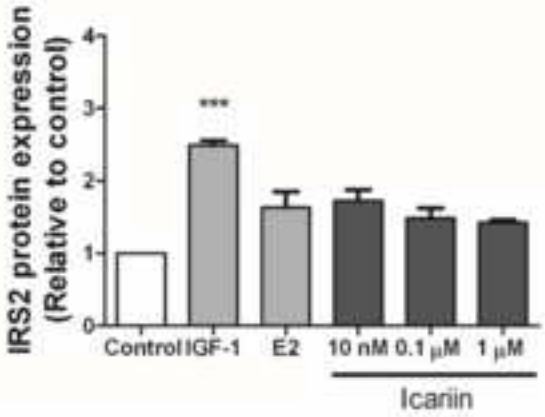


Figure 5

D

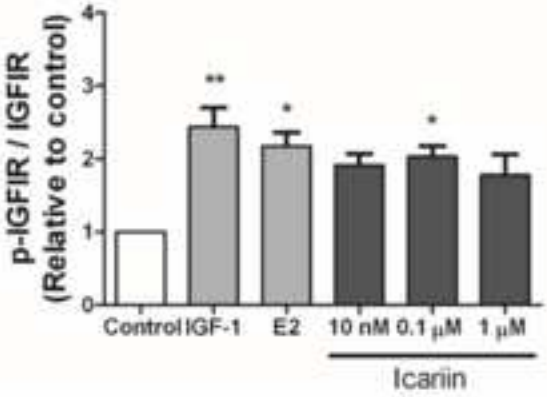


Figure 5

E

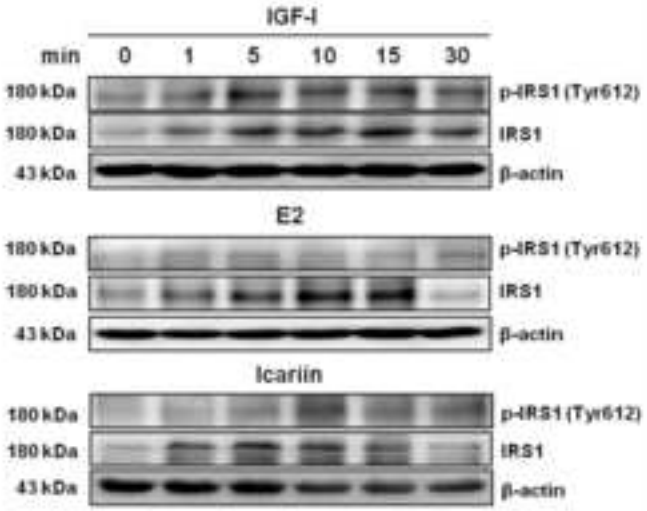


Figure 5

F

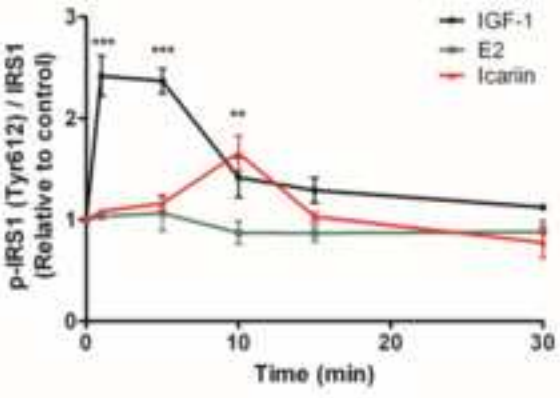

**Figure 6A-F**

Figure 6

A

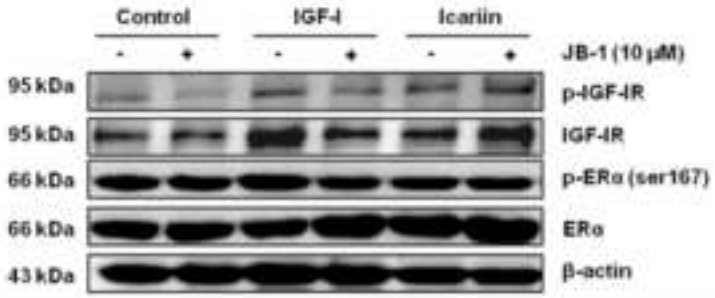


Figure 6

B

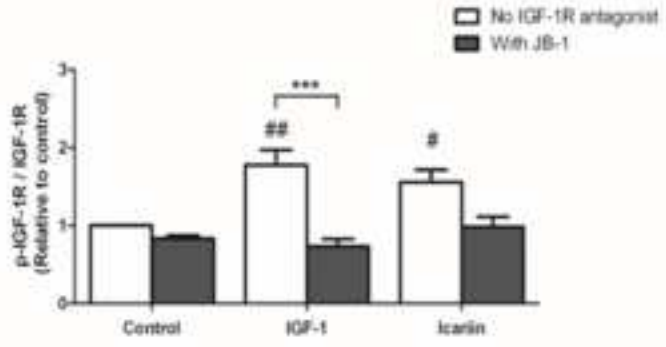


Figure 6

C

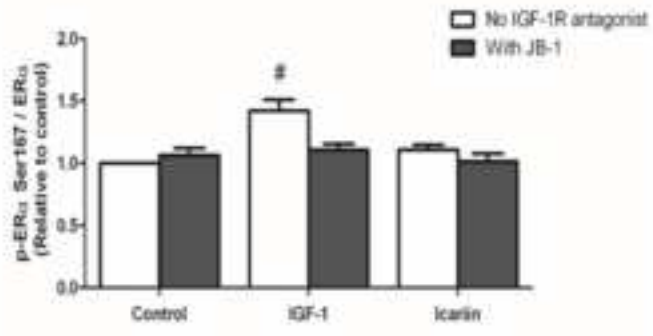


Figure 6

D

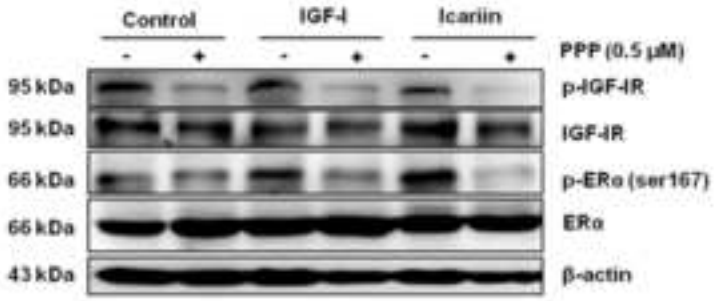


Figure 6

E

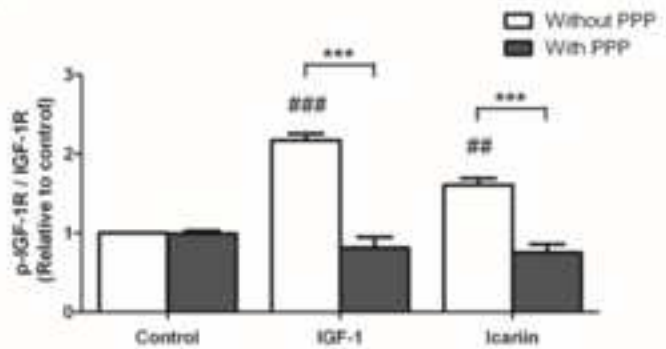


Figure 6

F

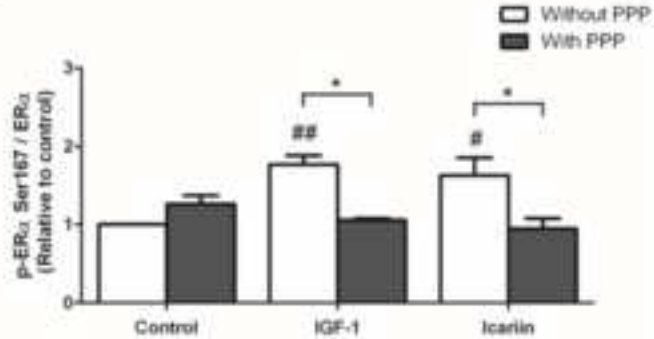

Figure 6G-H

Figure 6

G

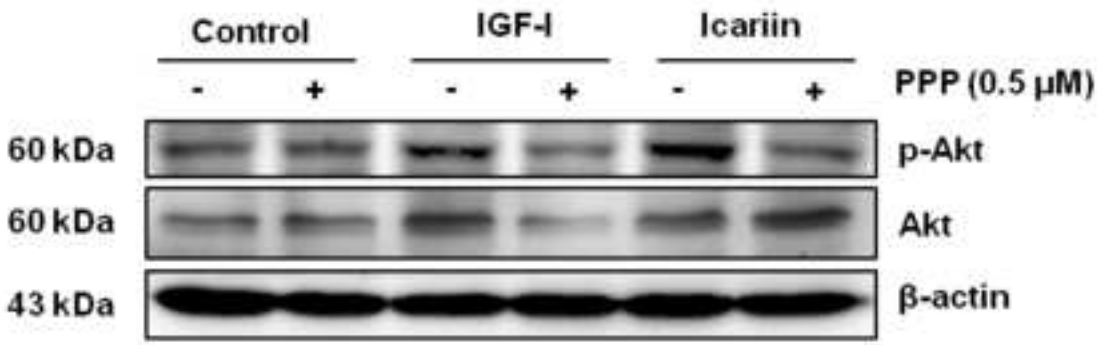


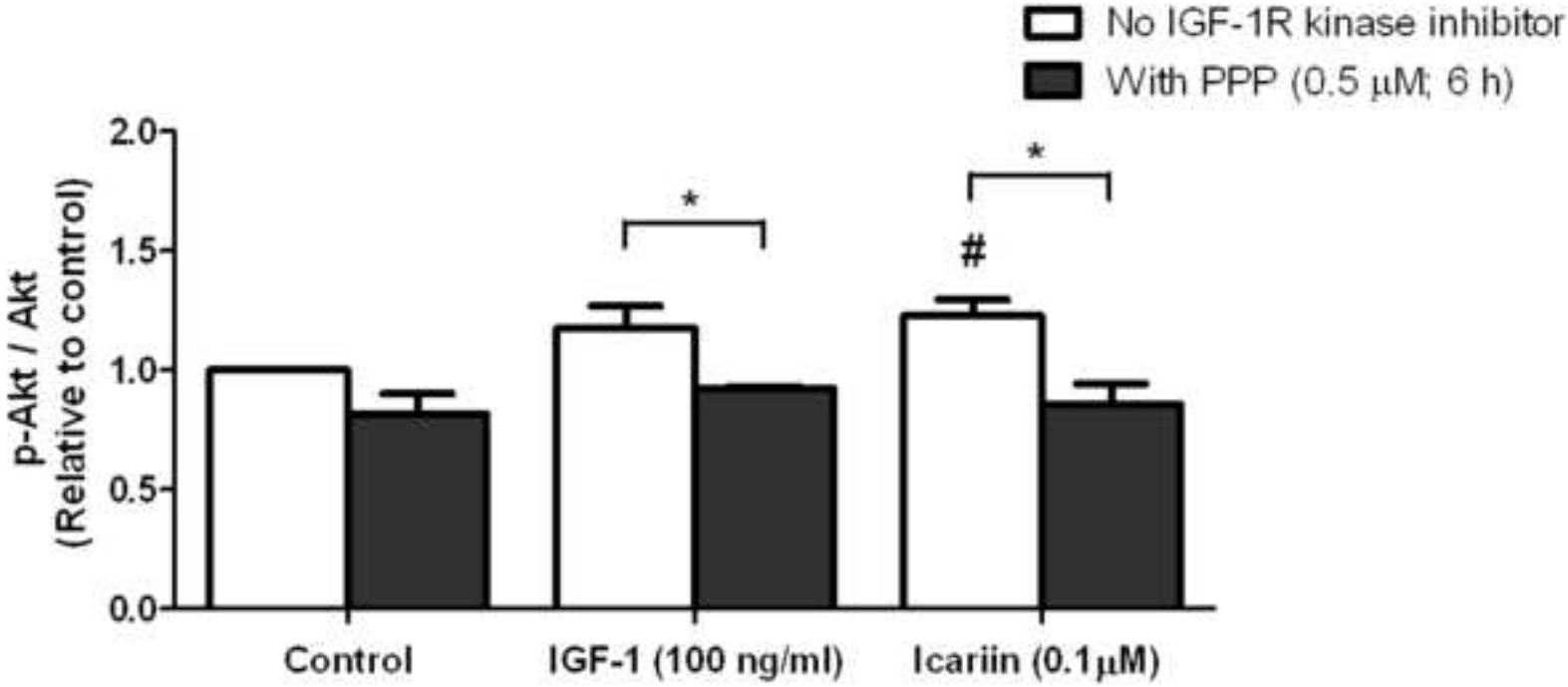

**Figure 6I and 6J**

Figure 6

I

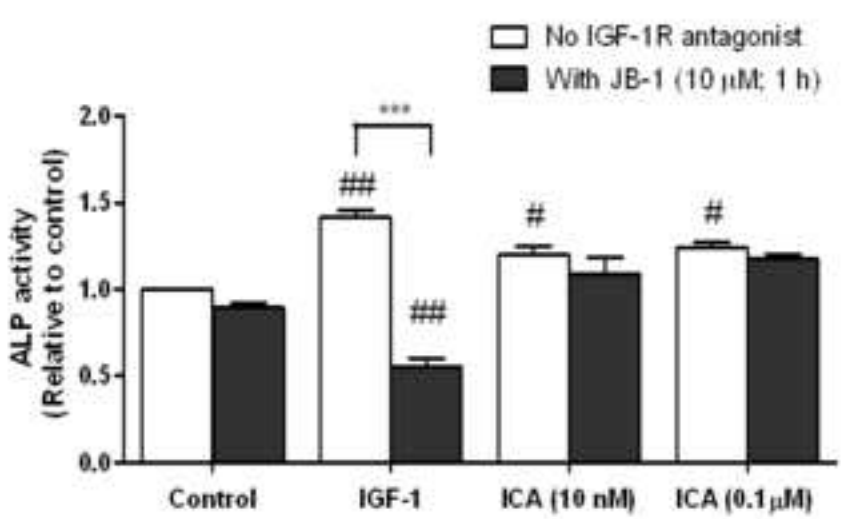


Figure 6

J

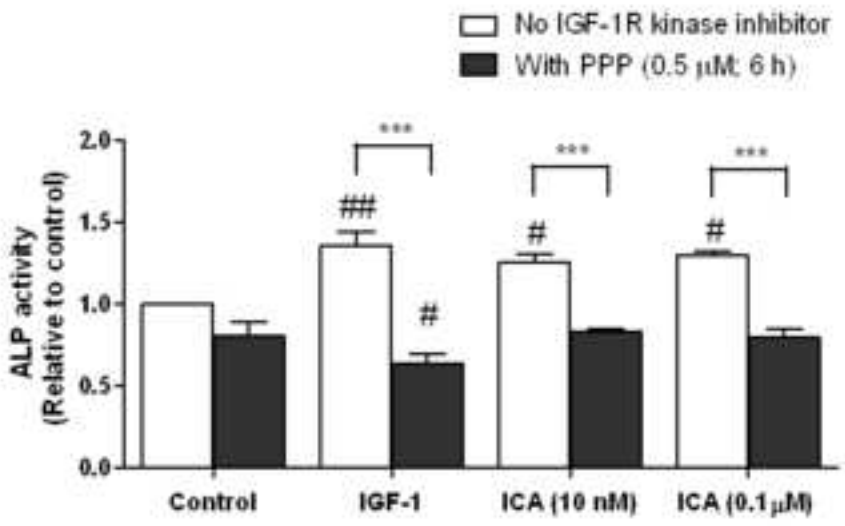

**Supplementary Figure 1**

Supplementary Figure 1

A

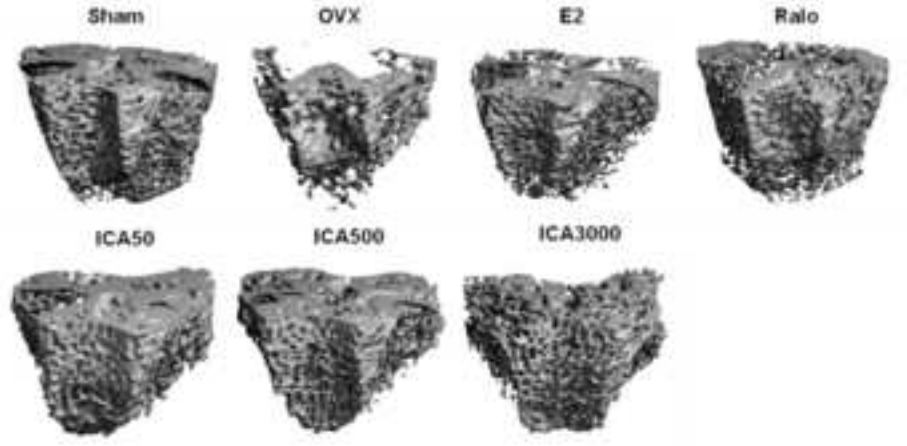


Supplementary Figure 1

B

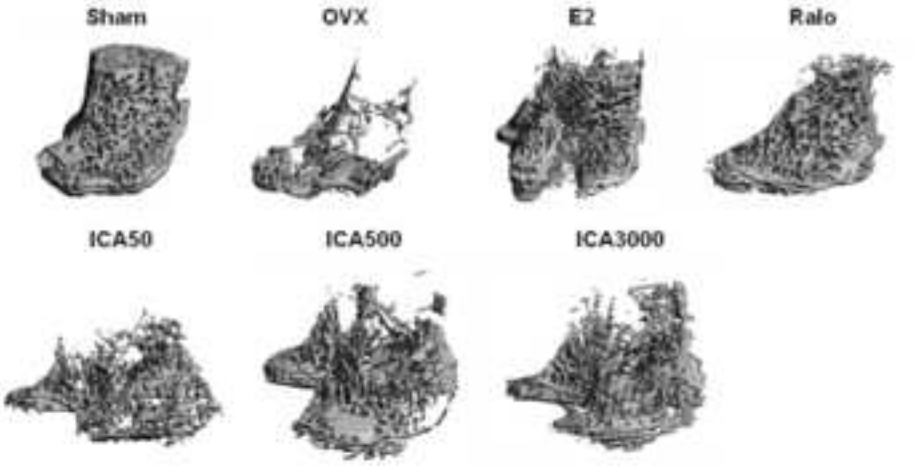


Supplementary Figure 1

C

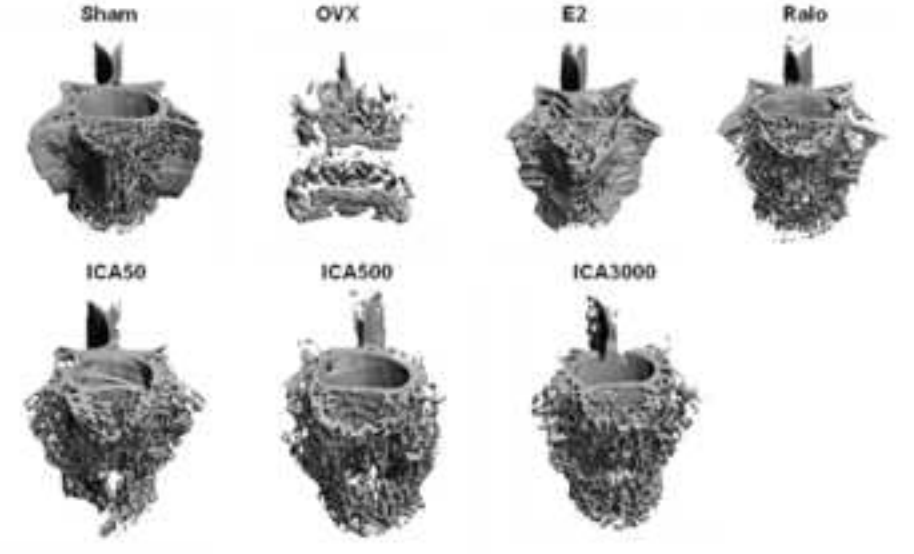

**Supplementary Figure 2**

Supplementary Figure 2

A

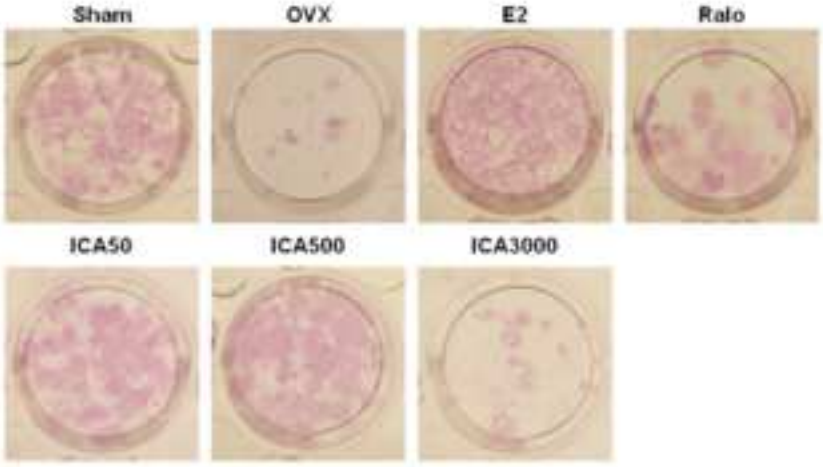


Supplementary Figure 2

B

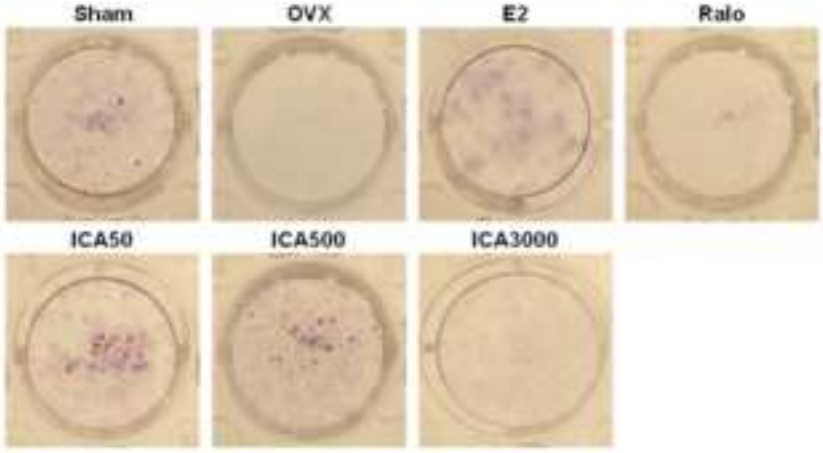


Supplementary Figure 2

C

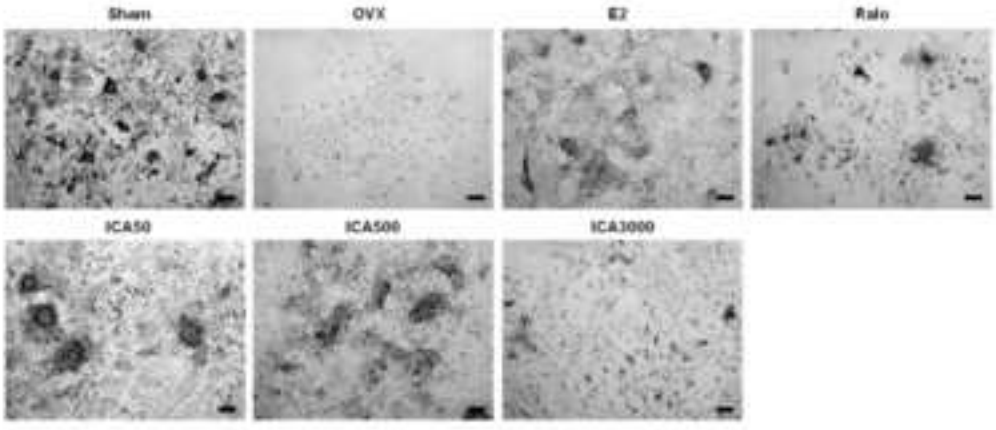

**Supplementary Figure 2D**

# Supplementary Figure 2

**D**

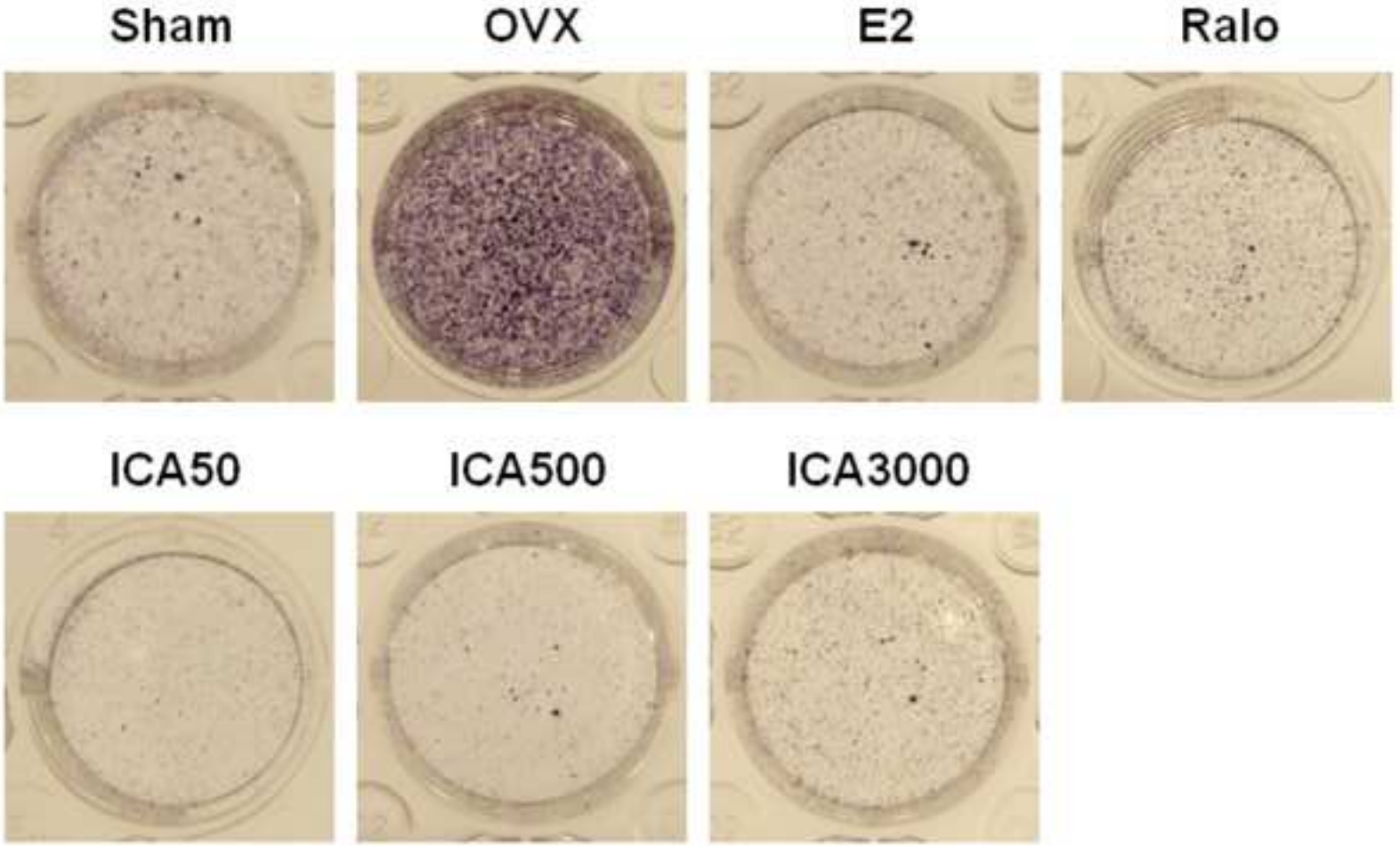

**Supplementary Figure 3**

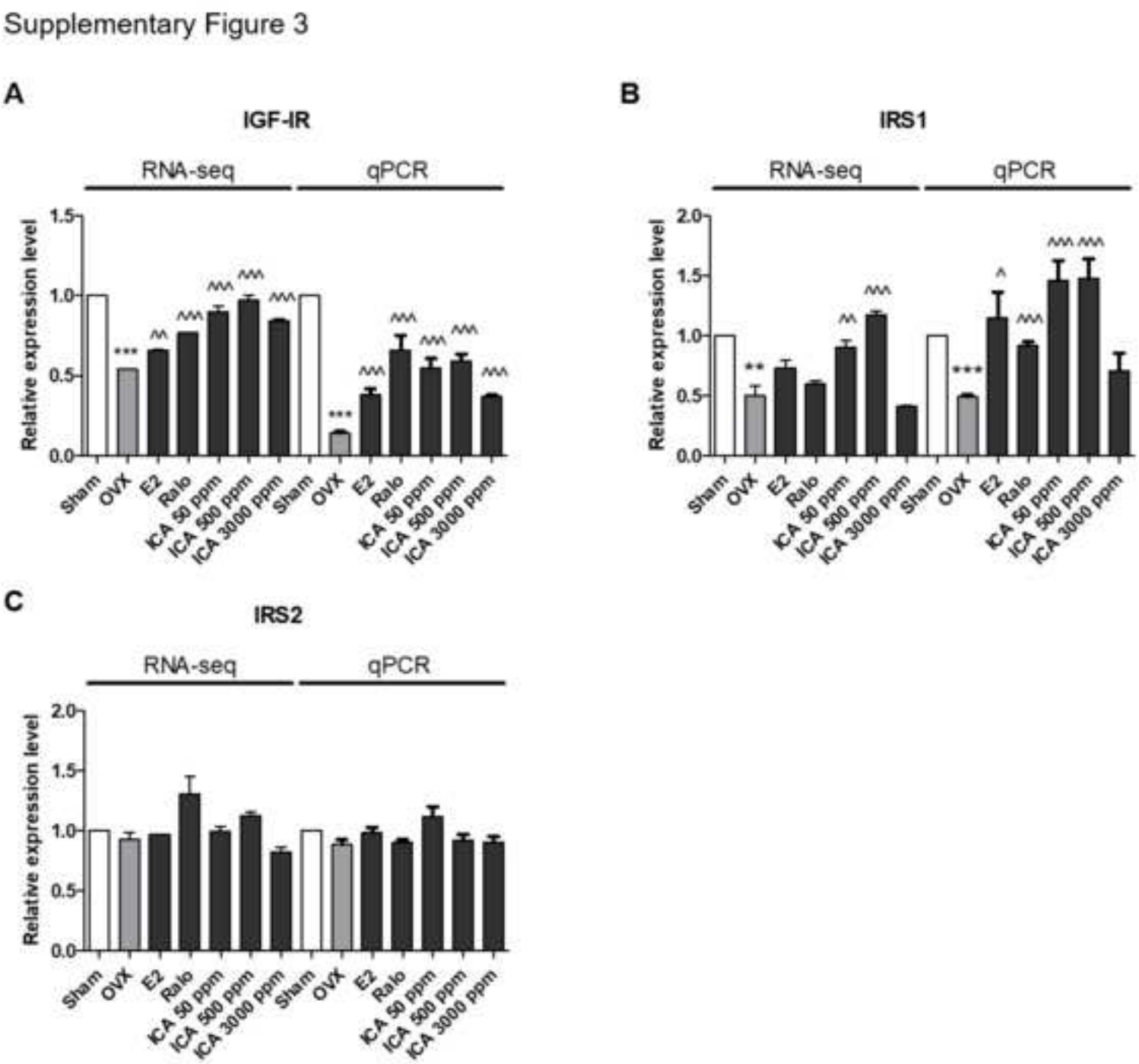

## Supplementary Table 1A

## Dose-dependent effects of icariin on trabecular bone properties at femur, tibia and lumbar vertebra in OVX rats

| | | Sham | OVX | E2 | Raloxifene | ICA50 | ICA500 | ICA3000 |
|---|---|---|---|---|---|---|---|---|
| Distal femur | BV/TV (%) | 54.3±2.94 | 10.7±0.50$^{***}$ | 34.0±1.07$^{\wedge\wedge\wedge}$ | 27.8±2.05$^{\wedge\wedge\wedge}$ | 22.6±1.62$^{\wedge\wedge}$ | 23.6±1.30$^{\wedge\wedge\wedge}$ | 24.6±2.57$^{\wedge\wedge\wedge}$ |
| | Tb.Th (mm) | 0.15±0.001 | 0.09±0.009$^{**}$ | 0.15±0.006$^{\wedge\wedge\wedge}$ | 0.13±0.005$^{\wedge}$ | 0.17±0.008$^{\wedge\wedge\wedge}$ | 0.16±0.009$^{\wedge\wedge\wedge}$ | 0.16±0.009$^{\wedge\wedge\wedge}$ |
| | Tb.N (1/mm) | 4.24±0.024 | 0.54±0.042$^{***}$ | 3.35±0.014$^{\wedge\wedge\wedge}$ | 2.79±0.053$^{\wedge\wedge\wedge}$ | 1.15±0.047$^{\wedge\wedge\wedge}$ | 1.16±0.057$^{\wedge\wedge\wedge}$ | 1.17±0.066$^{\wedge\wedge\wedge}$ |
| | Tb.Sp (mm) | 0.12±0.005 | 1.95±0.142$^{***}$ | 0.25±0.011$^{\wedge\wedge\wedge}$ | 0.26±0.007$^{\wedge\wedge\wedge}$ | 1.03±0.031$^{\wedge\wedge\wedge}$ | 0.96±0.037$^{\wedge\wedge\wedge}$ | 0.91±0.036$^{\wedge\wedge\wedge}$ |
| | Conn.D (1/mm$^3$) | 27.4±2.85 | 3.14±0.937$^{***}$ | 23.4±2.69$^{\wedge\wedge\wedge}$ | 18.0±2.28$^{\wedge\wedge\wedge}$ | 13.4±0.748$^{\wedge\wedge}$ | 13.7±1.02$^{\wedge\wedge}$ | 10.5±1.13 |
| | SMI | 1.67±0.116 | 2.78±0.148$^{**}$ | 1.55±0.125$^{\wedge\wedge\wedge}$ | 1.91±0.283$^{\wedge}$ | 1.76±0.188$^{\wedge\wedge}$ | 1.70±0.154$^{\wedge\wedge}$ | 1.63±0.191$^{\wedge\wedge\wedge}$ |
| Proximal tibia | BV/TV (%) | 52.4±0.58 | 5.8±0.60$^{***}$ | 32.6±1.72$^{\wedge\wedge\wedge}$ | 20.7±0.23$^{\wedge\wedge\wedge}$ | 11.3±0.84$^{\wedge}$ | 13.4±1.44$^{\wedge\wedge\wedge}$ | 16.8±2.44$^{\wedge\wedge\wedge}$ |
| | Tb.Th (mm) | 0.20±0.006 | 0.12±0.003$^{**}$ | 0.24±0.017$^{\wedge\wedge\wedge}$ | 0.20±0.004$^{\wedge\wedge\wedge}$ | 0.14±0.009 | 0.13±0.005 | 0.13±0.007 |
| | Tb.N (1/mm) | 4.60±0.123 | 0.37±0.065$^{***}$ | 3.08±0.135$^{\wedge\wedge\wedge}$ | 2.71±0.068$^{\wedge\wedge\wedge}$ | 0.83±0.048$^{\wedge\wedge}$ | 0.81±0.052$^{\wedge\wedge}$ | 0.92±0.068$^{\wedge\wedge\wedge}$ |
| | Tb.Sp (mm) | 0.05±0.011 | 1.22±0.082$^{***}$ | 0.25±0.016$^{\wedge\wedge\wedge}$ | 0.28±0.003$^{\wedge\wedge\wedge}$ | 0.21±0.127$^{\wedge\wedge\wedge}$ | 0.24±0.073$^{\wedge\wedge\wedge}$ | 0.31±0.088$^{\wedge\wedge\wedge}$ |
| | Conn.D (1/mm$^3$) | 25.5±0.084 | 4.67±0.574$^{***}$ | 17.2±0.764$^{\wedge\wedge\wedge}$ | 16.0±1.74$^{\wedge\wedge\wedge}$ | 11.8±1.17$^{\wedge\wedge\wedge}$ | 12.2±1.04$^{\wedge\wedge\wedge}$ | 12.0±0.792$^{\wedge\wedge\wedge}$ |
| | SMI | 1.47±0.111 | 2.20±0.244 | 1.31±0.196$^{\wedge}$ | 1.25±0.33$^{\wedge}$ | 1.60±0.113 | 1.49±0.058 | 1.54±0.080 |
| Lumbar vertebra | BV/TV (%) | 43.2±0.38 | 8.5±0.31$^{***}$ | 32.2±1.16$^{\wedge\wedge\wedge}$ | 33.5±1.66$^{\wedge\wedge\wedge}$ | 13.8±1.09 | 20.0±3.87$^{\wedge\wedge\wedge}$ | 15.1±0.01 |
| | Tb.Th (mm) | 0.16±0.001 | 0.11±0.002$^{**}$ | 0.26±0.010$^{\wedge\wedge\wedge}$ | 0.19±0.002$^{\wedge\wedge}$ | 0.16±0.015 | 0.17±0.011$^{\wedge}$ | 0.16±0.012$^{\wedge}$ |
| | Tb.N (1/mm) | 4.11±0.005 | 0.61±0.004$^{***}$ | 3.62±0.035$^{\wedge\wedge\wedge}$ | 3.54±0.056$^{\wedge\wedge\wedge}$ | 0.96±0.036$^{\wedge\wedge}$ | 1.07±0.089$^{\wedge\wedge\wedge}$ | 1.15±0.115$^{\wedge\wedge\wedge}$ |
| | Tb.Sp (mm) | 0.14±0.002 | 1.64±0.065$^{***}$ | 0.17±0.006$^{\wedge\wedge\wedge}$ | 0.18±0.002$^{\wedge\wedge\wedge}$ | 0.99±0.036$^{\wedge\wedge\wedge}$ | 0.89±0.063$^{\wedge\wedge\wedge}$ | 0.93±0.065$^{\wedge\wedge\wedge}$ |
| | Conn.D (1/mm$^3$) | 20.6±0.869 | 4.27±0.303$^{***}$ | 14.0±1.18$^{\wedge\wedge\wedge}$ | 13.8±1.12$^{\wedge\wedge\wedge}$ | 11.2±0.656$^{\wedge\wedge\wedge}$ | 12.8±0.498$^{\wedge\wedge\wedge}$ | 12.6±0.609$^{\wedge\wedge\wedge}$ |
| | SMI | 1.59±0.079 | 2.45±0.194 | 1.39±0.327$^{\wedge\wedge}$ | 1.33±0.313$^{\wedge\wedge}$ | 1.88±0.082 | 1.57±0.092$^{\wedge}$ | 1.74±0.119 |

**Supplementary Table 1B**

**Dose-dependent effects of icariin on cortical bone properties at femur, tibia and lumbar vertebra in OVX rats**

| | | Sham | OVX | E2 | Raloxifene | ICA50 | ICA500 | ICA3000 |
|---|---|---|---|---|---|---|---|---|
| Distal femur | BV/TV (%) | 20.3±2.6 | 13.1±1.3$^{*}$ | 21.9±1.5$^{\wedge}$ | 21.2±0.7$^{\wedge}$ | 23.2±0.5$^{\wedge\wedge}$ | 22.7±1.6$^{\wedge\wedge}$ | 21.1±1.3$^{\wedge}$ |
| | BMD (mg/cm$^3$) | 533.4±18.8 | 464.3±18.6 | 528.8±18.8 | 488.1±39.9 | 566.3±7.43 | 614.5±37.3$^{\wedge}$ | 587.4±25.0 |
| Proximal tibia | BV/TV (%) | 20.6±2.1 | 18.5±4.4 | 18.6±1.3 | 18.7±1.8 | 27.9±1.0 | 24.4±0.7 | 22.7±1.5 |
| | BMD (mg/cm$^3$) | 511.1±31.7 | 471.2±29.3 | 482.0±38.3 | 437.9±28.7 | 575.9±6.4 | 560.7±27.3 | 577.5±18.7 |
| Lumbar vertebra | BV/TV (%) | 10.3±0.6 | 5.33±0.3$^{**}$ | 9.7±1.4$^{\wedge}$ | 8.8±0.1 | 8.9±1.1 | 8.6±0.8 | 7.8±0.6 |
| | BMD (mg/cm$^3$) | 438.4±27.8 | 345.0±15.7 | 419.6±36.5 | 393.3±36.6 | 414.6±37.7 | 378.3±12.9 | 343.0±23.2 |

**Supplementary Table 2**

**Summary of RNA sequencing data for each sample.**

| Samples | Clean reads | Clean bases | GC content | %≥Q20 |
|---|---|---|---|---|
| Sham | 23,905,643 | 1,195,282,150 | 58.81% | 92.9% |
| OVX | 23,833,306 | 1,191,665,300 | 63.05% | 93.4% |
| EST | 24,010,919 | 1,200,545,950 | 58.38% | 93.6% |
| RAL | 23,723,047 | 1,186,152,350 | 58.00% | 94.1% |
| ICA50 | 24,006,109 | 1,200,305,450 | 58.10% | 94.1% |
| ICA500 | 22,810,239 | 1,140,511,950 | 60.77% | 93.6% |
| ICA3000 | 23,903,758 | 1,195,187,900 | 64.37% | 93.4% |

**Author statement:**

**Man-Sau Wong and Yan Zhang:** Conceptualization, Methodology. **Liping Zhou, Christina C.W. Poon, Ka Ying Wong and Sisi Cao:** Investigation, Validation. **Liping Zhou and Christina C.W. Poon:** Formal analysis, Visualization and Writing – Original draft preparation. **Xiaoli Dong**, **Yan Zhang and Man-Sau Wong:** Writing – Review & Editing. **Man-Sau Wong and Yan Zhang:** Supervision and Funding acquisition.